ARTICLE

https://doi.org/10.1590/2317-4889202320220040

BJGEO
Brazilian Journal of Geology

Remote sensing applied to geological, structural, and mass movements characterization in the connection between Curral Homocline and Moeda Syncline, Quadrilátero Ferrífero Region, Brazil

Jorge Roncato[1]*, Marina Morena Martins[1], Matheus Marlley Lacerda Silva[1]

Abstract

Mass movements naturally occurring along slopes, especially after heavy rains, cause heavy losses of materials and life and affect highways, pipelines, and bridges, among other structures. Among the most common mass movements, landslides and subsequent mass flows especially stand out. Remote sensing and geoprocessing techniques are useful tools for geological and geotechnical analysis, here applied to characterization of mass movements from the analysis of the influence of slopes, lineaments or fractures, and geological-geotechnical at the junction of the Curral homocline and the Moeda syncline, Quadrilátero Ferrífero, Southeast Brazil. The area consists of Archean granitic-gneissic basement and the greenstone belt sequence of the Rio das Velhas Supergroup with Proterozoic metasedimentary rocks of the Minas Supergroup covering these two older successions. Based on satellite images, a preliminary map of lineaments was created, and fractures were grouped according to their direction before being rasterized. Each lineament group was associated with a previously known geological and/or structural feature. Geological units mapped in the area were numerically classified according to their mass movement susceptibility and related geotechnical units. Using a Shuttle Radar Topography Mission (SRTM) image, a terrain slope raster was generated. The objective was to obtain a raster indicating low and high probabilities of mass movements. Four sets of lineaments were identified: the first set associated with the northeast strike stratification of the rocks of the Moeda Formation; the second set related to eastward-trending warp axis lineations; the third set related to the southeast trend of stretch lineaments or mafic dykes directions; and the fourth set evidently associated with the watershed pattern of the Curral Range crest, perpendicular to the strike of the rocks in the area. Simulations with different combinations of parameters produced eight scenarios were generated were constructed to classify the area as to its susceptibility to rupture through changes in slope, lithotype, and lineament density; the first four (1 to 4) were classified by using the slope percentage raster without interval reclassification, so its values in the cartographic algebra were not grouped. The last for (5 to 8), consider the slope percentage classified. This methodology successfully combines mathematical models for predicting mass movements and determining areas in the urban landscape most susceptible to these phenomena. As such, it comprises a useful tool for government planning of preventative actions for areas of high risk.

KEYWORDS: mass movement; remote sensing; geological mapping; Quadrilátero Ferrífero; multicriteria analysis methods; conceptual geotechnical model.

INTRODUCTION

Brazil, due to its climatic conditions and large mountain ranges, is very susceptible to the occurrence of mass movements. In addition to the high frequency of accidents caused by natural conditions, there are also a large number of accidents associated with human activities on the slopes. Among the human actions that are most concerned in Brazil, the irregular occupation of the slopes by suburbs and settlements stands out, which ends up making cuts in the slopes and causing deforestation, providing a greater susceptibility to the occurrence of mass movements.

Thus, it becomes essential not only for the prediction of landslides, which are closely linked to their occurrence on the slopes, but also for the prediction of the reach and deposit of mass movements, and with that, to guide, help, and anticipate the responsible organs in the areas susceptible to these events. A variety of methodologies have been developed in the prediction analysis, such as those based on the analysis of geological lineaments, regional and local geological structures, and transported material deposits to delineate the areas critical to the occurrence of mass movements. Its distribution in the field suggests future patterns of instability in the relief, the methodologies that make risk maps from the combination of different types of information plans (e.g., geology; presence, or not, of vegetation; land use; slope; and geological structures) in which, "weights" and/or "grades" are given for each attribute (information plane), identifying its degree of importance for the mass

[1]Instituto de Geociências, Departamento de Geologia, Universidade Federal de Minas Gerais – Belo Horizonte (MG), Brazil.
E-mails: roncato@ufmg.br, matheusmarlley111@hotmail.com, marinamorenamartins@gmail.com

*Corresponding author.

movement (e.g., Seeley and West 1990, Xavier da Silva *et al*. 1996, Moreira 1999).

The use of models is linked to the very use of the scientific method as a process that employs previous experiences as a basis for predicting the future state of any physical system (Christofoletti 1999). The models try to simulate or represent in a simplified way the process or phenomenon of a certain environment and, from that, try to predict it. Through modeling, we can test ideas and hypotheses and carry out prediction studies. Models are used to describe, explore, and analyze how a system works. These models are based on the inherent laws of nature in that they try to represent natural mechanisms through mathematical equations. In this context, the general objective of this work is to develop a methodology that combines mathematical models of landslide prediction and mass movement to determine in the landscape the test area chosen for being more susceptible to the occurrence of these phenomena. In this way, it is also intended to suggest areas susceptible to mass movement through a mathematical forecast model.

Landslide occurrence can vary depending on different causes such as geology, topography, tectonic history, weathering, and land use. Moreover, the triggering of mass movements can be due to a variety of factors both natural, such as rainfall, earthquakes, and water level changes, and anthropogenic (Rosi *et al*. 2013). Good knowledge of mass movement behavior is required to reduce the risk posed by such phenomena. The understanding of regional-scale geological structures can indicate regions of weakness susceptible to mass movements. Recent studies have attempted to constrain the unknown parameters of folding at various field sites, making use of mechanical models for which the present-day fold shape and fracture distributions serve as calibration (e.g., Shamir and Eyal 1995, Zhang *et al*. 2000, Johnson and Johnson 2002, Savage and Cooke 2004, Bellahsen *et al*. 2006; and references therein). In the widely published bibliography, knowledge of the fracture patterns in fold structures is limited. The systematic (planar, parallel, repetitious) fracture sets were decreased as 'of compressional deformational origin' and 'related to shear stresses' (Bellahsen *et al*. 2006), and this diagnostic evidence was apparently based purely on the geometry of the fracture sets.

Some studies (e.g., Sanderson 1982, Hedlund *et al*. 1994, Storti and Salvini 1996, Salvini and Storti 2001, Tavani *et al*. 2008, Nabavi and Fossen 2021) suggested that structural (i.e., geometrical and kinematical) variables control the final deformation pattern in the fold. The study area is located in the connection between two large regional structures, whose plane-axial foliation planes directly interfere with the development of slopes and scarps, which have different susceptibilities to mass movements.

Google Earth Pro (GEP) and QGIS proved to be highly effective tools for the identification and mapping of lineament patterns on the crests and limbs of these geological structures, as well as for other fold-related structural applications. The platforms used do not allow for the analysis of 3D information on the fracture sets; these data must be collected from the outcrop. Therefore, GEP is not a replacement for boots-on-the-ground fieldwork (Lageson *et al*. 2012).

In this article, aerial and radar data from the area of connection between the Curral homocline and Moeda syncline are presented. This site consists of a fracture model and geometry at the macro- and mesoscale that describe the structural and stratigraphic influences on the deformation pattern. The objective of this study was to apply the knowledge to the GEP mapping and interpretation of lineament patterns on regional geological structures in the Quadrilátero Ferrífero region and their relationship with mass movement events. Another intention was to become familiar with the mapping tools of GEP and compatible software applications for descriptive structural analysis, such as landslide occurrence, explore the possibilities of GEP for other applications in structural geology, and apply the aforementioned techniques based on the study of Lageson *et al*. (2012).

To increase this knowledge, a complete analysis of the geological setting, geotechnical properties, and triggering factors of mass movements are necessary, even as a controlled description and interpretation of lineament patterns on the connection between two important ridges of Quadrilátero Ferrífero region (Figs. 1 and 2).

REGIONAL GEOLOGICAL SETTING

Geological context

The Quadrilátero Ferrífero region (Figs. 1 e 2) is situated in the southern portion of the São Francisco craton (Almeida *et al*. 1976) and is composed of the Archean Rio das Velhas greenstone belt (Schorscher *et al*. 1982), the Paleoproterozoic Minas Supergroup, and the Itacolomi Group. These supracrustal units are surrounded by granite-gneiss domes (Dorr 1969, Lana *et al*. 2013), which consist of the poly-deformed unit. The regional basement metamorphic complexes outcrop in distinct domes, with metamorphic grades ranging from greenschist to granulite metamorphic facies (Herz 1970).

The investigated area is located in the northern portion of Moeda Ridge, the central portion of the Quadrilátero Ferrífero Region, locally known as Rola-Moça State Park. This region (Fig. 1) was chosen for the investigation because it contains the connection between the Curral homocline and Moeda syncline, a poorly studied area. Even though the Quadrilátero Ferrífero is a widely known and studied region, that specific site exhibits a complex structural pattern.

The Quadrilátero Ferrífero region can be subdivided into four Archean and Paleoproterozoic lithostratigraphic units:

(i) Archean metamorphic complexes composed of gneisses, migmatites, and granitoids;
(ii) the Archean Rio das Velhas Supergroup, formed by low-to-medium grade metavolcanic and metasedimentary rocks; (iii)
(iii) the Neoarchean and Paleoproterozoic Minas Supergroup, consisting of low-to-medium grade metasedimentary rocks;
(iv) the Paleoproterozoic Itacolomi Group composed of metasandstones and conglomerates (e.g., Dorr II *et al*. 1957, Dorr 1969, Cordani *et al*. 1980, Schorscher *et al*.

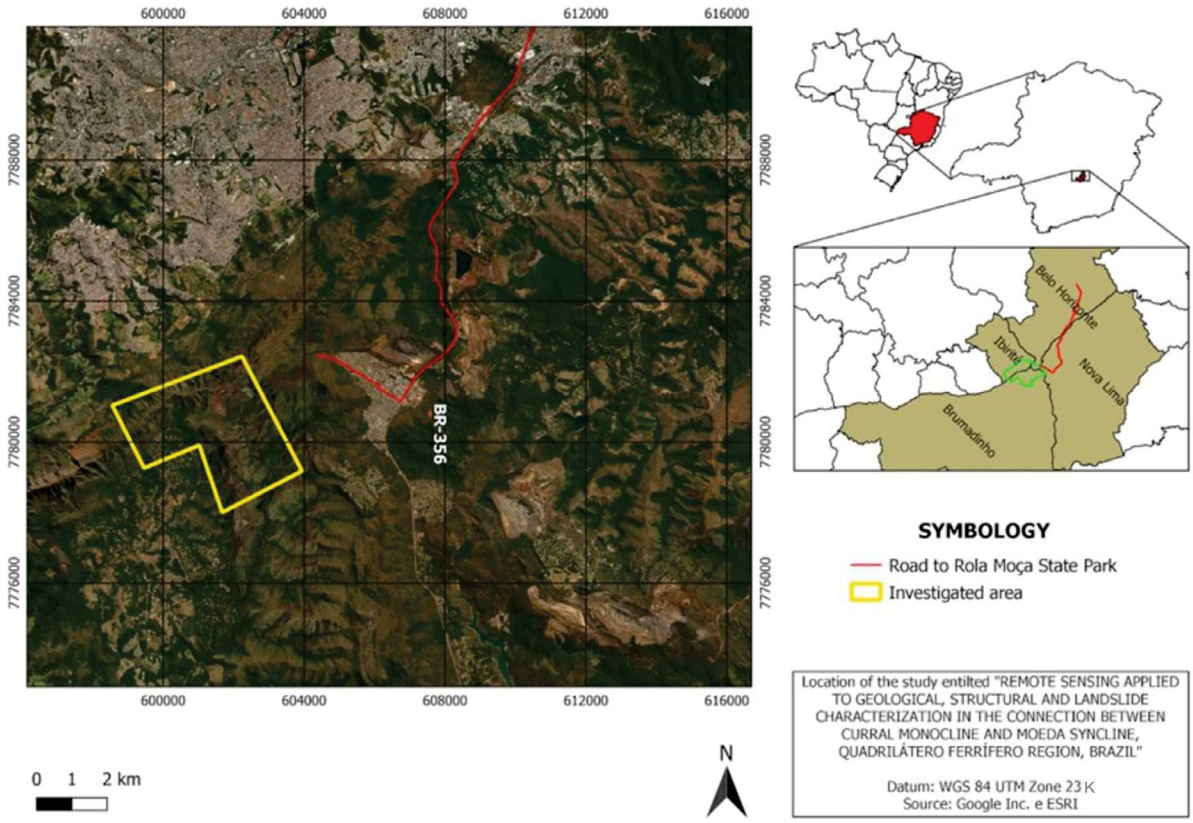

Figure 1. Location of the study area.

1982, Romano 1989, Noce 1995, Machado *et al.* 1996, Endo and Machado 1997, Lana *et al.* 2013, Farina *et al.* 2016, Dutra 2017, Roncato *et al.* 2020).

The Rio das Velhas greenstone belt corresponds to a meta-volcano sedimentary sequence composed from the base to the top by the Nova Lima and Maquiné groups, respectively (Dorr *et al.* 1957, Schorscher 1982). The Nova Lima Group comprises a basal unit formed by tholeiitic-komatiitic volcanic rocks, associated with chemical sedimentary rocks; a volcaniclastic intermediate unit, associated with felsic volcanism; and an upper unit with clastic sedimentary rocks (Ladeira 1991, Zucchetti and Baltazar 2000, Baltazar and Zucchetti 2007). Schorscher (1982) described komatiites at the base of the sequence, naming them the Quebra Osso Group. The Maquiné Group, shown in Fig. 2, is composed of sequences of graywacke and conglomerates (Gair 1962, Moreira *et al.* 2016).

The stratigraphic subdivision of the Rio das Velhas greenstone belt based on lithofacies associations by Zucchetti and Baltazar (2000) and Baltazar and Zucchetti (2007) is used in this contribution. From the base to the top, these are:

(i) mafic-ultramafic volcanic;
(ii) volcano-chemical sedimentary;
(iii) clastic-chemical sedimentary;
(iv) volcaniclastic;
(v) resedimented (hereafter renamed clastic sedimentary association), widely distributed in the QF, comprising mainly graywackes, quartz graywackes, and siltstones, with the indication that it was deposited by turbidity currents of high and low densities;
(vi) coastal and non-marine associations.

As summarized by Roncato *et al.* (2015) and Roncato *et al.* (2020), about Minas Supergroup, this 2.60–2.10 Ga (Machado *et al.* 1996, Hartmann *et al.* 2000) unit is subdivided into the Caraça, Itabira, Piracicaba, and Sabará Groups (Dorr 1969), all metamorphosed at low greenschist facies. The basal Caraça Group has metaconglomerate, quartzite, and phyllite (Renger *et al.* 1994). The Itabira Group includes the Cauê Formation that hosts a great volume of Superior-lake BIF and iron orebodies in the region (Rosière *et al.* 2008). The Piracicaba Group is formed by phyllites and quartzites. The Sabará Group unconformably overlies the Piracicaba Group, and its deposition is considered about 2.12 Ga (Machado *et al.* 1996); it is a flysch sequence with metagraywacke, carbonaceous phyllite, metadiamictites, metaconglomerates, and felsic to intermediate metavolcanic rocks (Dorr 1969). The Itacolomi Group (Dorr 1969) is the youngest unit in QF, resting unconformably on the Minas Supergroup, and contains quartzite, metarkose, and metaconglomerate.

According to the review of Dorr's (1969) lithostratigraphic column proposed by Endo *et al.* (2020), the Estrada Real Supergroup comprises the Sabará and Itacolomi groups, representing the youngest units and the top of the stratigraphic section of the Quadrilátero Ferrífero region. The repositioning proposed is consistent with the fact that the depositional environment and source areas of the Sabará Group's rocks are different from those

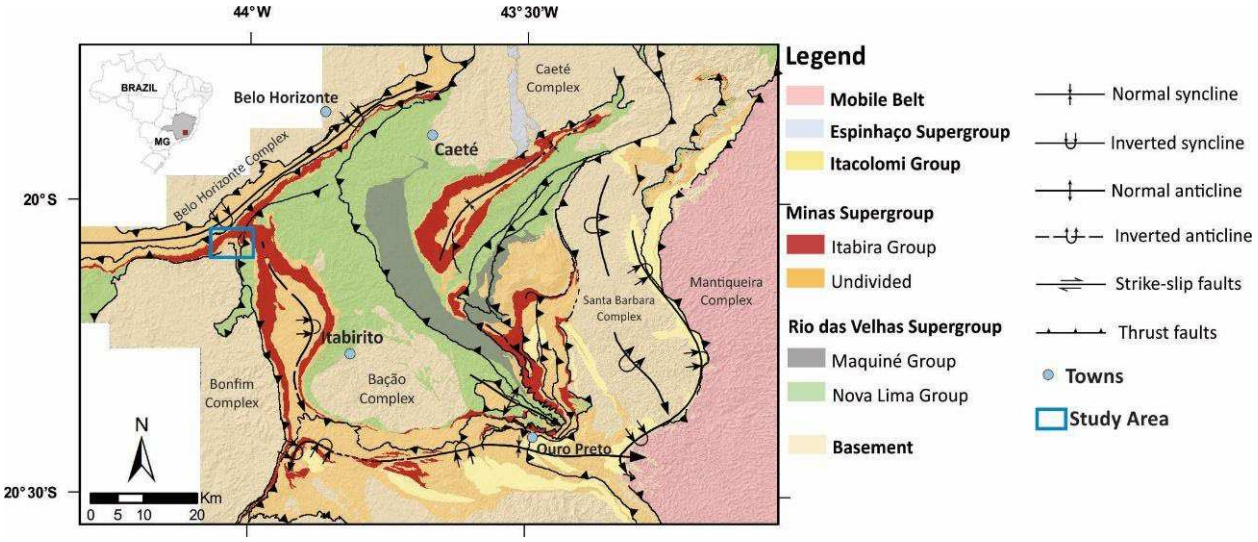

Source: after Costa (2022).
Figure 2. Simplified geological and structural map of the Quadrilátero Ferrífero region.

of the Minas Supergroup (Almeida *et al.* 2005). The contact between the Minas Supergroup and the Estrada Real Supergroup is marked by an erosive disagreement (Dorr 1969).

The structural evolution of the QF region took place in three main periods during the Rio das Velhas Orogeny (Baltazar and Zucchetti 2007): between 2.8 and 2.67 Ga, which relates to the evolution of the Rio das Velhas greenstone belt; from 2.10 to 1.90 Ga, the Transamazonian event; and the Brasiliano orogeny (Roncato 2016, Sepulveda *et al.* 2021).

According to Alkmim and Marshak (1998), the Proterozoic tectonic evolution (Minas accretionary orogeny of Teixeira *et al.* 2015, from 2.35 to 2.00 Ga) took place in three main deformational phases. Fold and thrust belt shortly after 2.125 Ga; orogenic collapse with the uplift of Archean granite-gneiss domes and formation of regional synclines at 2.09 Ga (Marshak and Alkmim 1989); and the Brasiliano orogeny (0.7–0.45 Ga), with fold and thrust belts verging to the west. Published U-Pb ages data from the basement of the QF allowed for the identification of four main magmatic events (Lana *et al.* 2013, Romano *et al.* 2013, Farina *et al.* 2016). Periods of magmatic activity, which register the tectonomagmatic Archean history of the QF, were described as the Santa Bárbara, Rio das Velhas I, Rio das Velhas II, and Mamona.

The QF region has a geometry delineated by synform and antiform mega folds that, in its eastern portion, are truncated by north-south thrust faults (Baltazar and Zucchetti 2007). Alkmim and Marshak (1998) described a dome-and-keel structure, in which the basement occurs as domes (e.g., Bação, Bonfim, and Santa Bárbara) that are circled by keels containing rocks of the Archean Rio das Velhas greenstone belt and the Minas Supergroup.

Geology of the connection between Curral homocline and Moeda syncline area

The Serra do Rola-Moça State Park is located at the confluence of two great lineaments (Curral and Moeda) and the most typical rocks of Quadrilátero Ferrífero region stratigraphy (Fig. 2) sustain the geomorphology of this area (Pereira *et al.* 2013). The Curral Ridge is a homocline and is located in the northern region striking east-west, while the Moeda Ridge is a syncline located in the western region striking north-south.

The set of reliefs is mostly mountainous and strongly oriented, marked by an approximately square system of ridges formed by quartzites and itabirites, products of differential erosion, in addition to depressions consisting of granites, gneisses, and shales (Medina *et al.* 2005; Fig. 3). Are noticeable, detrital-lateritic coverings on the tops of planed surfaces. Their great resistance to physical and chemical weathering makes them persistent and different from different slope levels. These latter are related to the laterization of colluviums and talus, resulting from the mechanical breakdown of the summit surfaces or the itabirite ridges (Tricart 1961).

The Curral homocline is characterized by three distinct features: Itabirites covered by armor and with parallel ridges and ravines in the upper portion; dolomitic rocks with flattened plateaus in the intermediate portion; and phyllites associated with quartzites with low declivity hills in the lower portion (Minas Gerais 2007, Madeira 2018).

Bonfim Complex

The Bonfim Complex occurs in the southern portion along the tectonic contact with Moeda Formation (Madeira 2018). The main lithologies observed in this unity are granitic and trondhjemitic gneiss, basaltic amphibolite, tonalite, granite, and basaltic to andesitic diabase/metadiabase metamorphosed in amphibolite facies; sometimes they have a retrometarmorphic paragenesis, expressing a physicochemical re-equilibrium (Carneiro 1992).

The rocks generally show an N-S milonitic foliation and gneissosity, with some retaining igneous original texture. The contacts with overlying unities occasionally show kinematic indicators, which imply a tectonic inversion (Carneiro 1992).

Undivided Nova Lima Group

The Nova Lima Group occurs in a small area in the southeastern portion in contact with Moeda Formation (Madeira 2018).

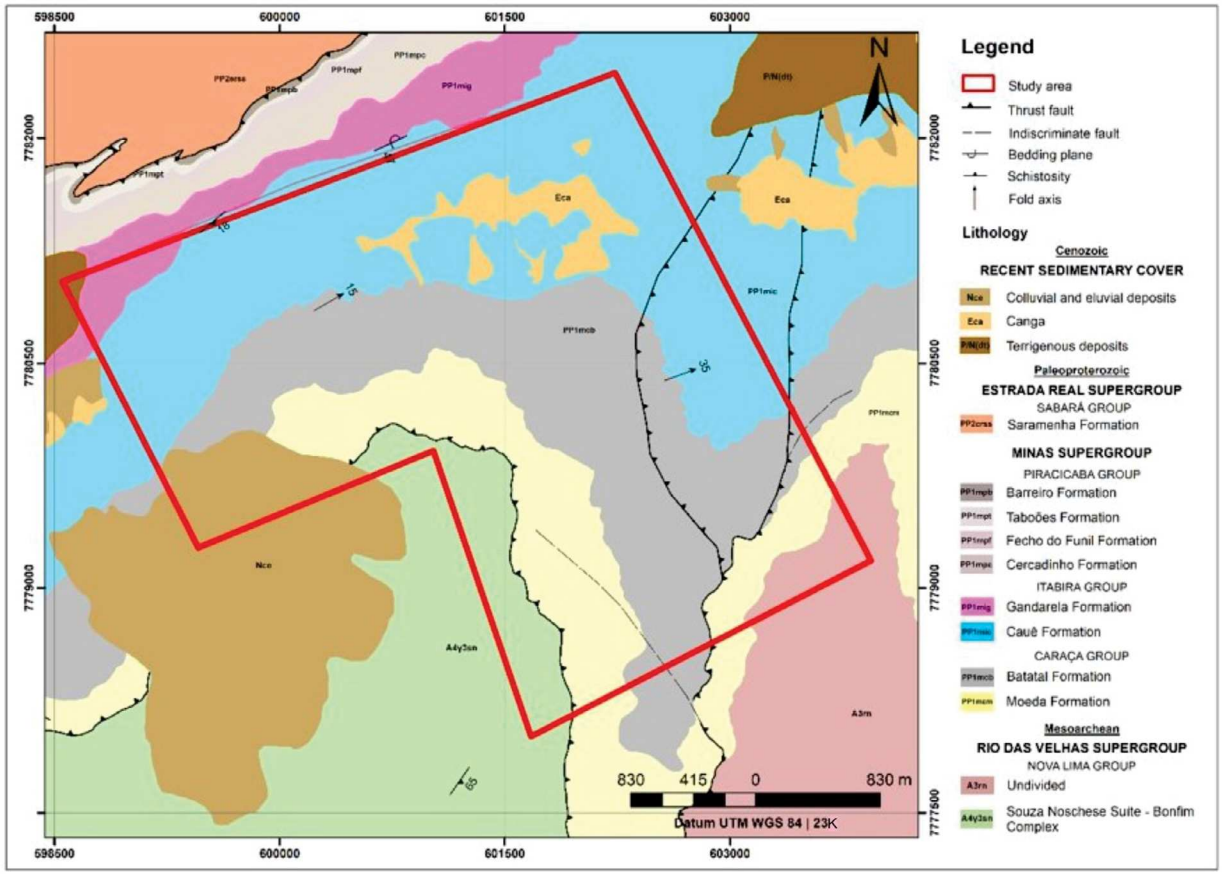

Source: modified from Endo *et al.* (2019).
Figure 3. Geologic map of the connection between Curral homocline and Moeda syncline area.

According to Baltazar and Zucchetti (2007), the Group consists of basic to ultrabasic volcanic rocks, metapelites, metacherts, BIF, metagreywackes, carbonaceous metapelites, acid to intermediate metavolcaniclastic rocks, and turbidites. Its contact with TTG basement is tectonic.

Caraça Group

Moeda Formation

The Moeda Formation is surrounded by Bonfim Complex, Nova Lima Group and Batatal Formation rocks. It is formed by quartzites with intercalations of phyllite and alluvial conglomeratic lenses randomly distributed, whose source is associated with the Rio das Velhas Supergroup (Dorr 1969, Noce 1995). The Moeda Formation is marked by the quartz composition in both lithologies and the presence of iron oxides between shear and bedding planes (Dorr 1969, Madeira 2018).

Batatal Formation

The Batatal Formation consists predominantly of phyllites, in addition to banded iron formations, metacherts, graphite phyllites, and dolomitic marbles (Dorr 1969, Madeira 2018, Endo *et al.* 2020). The rocks of this formation are easily weathered and have low resistance, so that, despite representing a thick package in the regional stratigraphy, they do not outcrop in the same way (Dorr 1969).

Itabira Group

Cauê Formation

In gradational contact with the Batatal Formation, the rocks of the Cauê Formation are superimposed (Dorr 1969, Noce 1995, Madeira 2018). This unit is characterized by the occurrence of itabirites, dolomitic itabirites, amphibolitic itabirites, and subordinately, small phyllite, quartzite, and marble lenses. The itabirites of the Cauê Formation are the main rocks that form the ridges in the relief of the study area, since their alteration products, the cangas, are very resistant to weathering (Dorr 1969).

Gandarela Formation

The Gandarela Formation has a gradational contact with the Cauê Formation (Madeira 2018). It is composed of large strata of calcitic and dolomite dolomites, such as dolomitic phyllites and ferruginous dolomites, in addition to thin layers of itabirite and intraformational metaconglomerates, which are constituted by tabular fragments of metachert and dolomites in a dolomitic matrix (Dorr 1969).

METHODS

This area was selected for this study because of its structural position, which is well displayed in Google Earth Pro (GEP), lack of any vegetation cover, and readily mappable

linear features. Google Earth Pro, *via Add Path, Show historical imagery*, and *Vertical exaggeration* functions, was considered for this project because of the ability to save excellent quality images for subsequent use.

Linear features and other geological features were identified by topographic maps and digital elevation models derived from NASA (2013), and satellite images (Google Earth and ESRI images). Even as Lageson *et al.* (2012), the lineaments measured are expressed as *lines* on bedrock dip-slopes and do not represent topographic features like ridgelines or stream channel terraces, although some joints are certainly exploited and widened by geomorphic processes. The authors performed all techniques and model applications. Except for the parameters used in Table 1, modified from the aforementioned study.

Google Earth Pro Methods

Google Earth Pro software was a fundamental tool for identifying features under high-resolution views in the focus area. With a combination of satellite images from diverse sources, aerial images, and 3D GIS, the program can provide precise visual data, which is responsible for conducting the outline of the lineaments that guided this project. The lines were initially identified under vertical perspective in two dimensions with a scale of 1:25,000. After a first analysis, the scale was increased to 1:10,000 under oblique perspective and a three-dimensional view. By alternating views at both scales, the lines were traced and numbered using the path *addition tool*. The criteria adopted were visual perceptions of positive and negative relief lines, in addition to roughness and textural recurrences. The lines searched had an average length of 110 m, with a wide standard deviation according to persistence.

QGIS Methods

The lines drawn in Google Earth Pro were exported to the QGIS software in order to promote the treatment of data and relate them to other images collected in previous stages. Once imported, the lineaments were analyzed using the *Attribute Table* tool, which relates each numbered trace to its linear dimension. To obtain azimuth information from each lineament, the following expression was used in the *Open Field Calculator: line_interpolate_angle($geometry,0)*. This function extracts the orientation from a linear feature, hereby expressed as "$geometry" and the last parameter, represented as "0", indicates the cardinal point reference, once 0 is north and 180 is south. The expression values and the results obtained are given in degrees. Also, lineaments length was obtained by using *$length* expression. By using Microsoft Excel, histograms were generated with the information listed in the *Attribute Table*, providing statistical results of mean, median, maximum, and minimum length values with a sample space equal to the totality of lines previously drawn. The spatial analysis was based on the regional map (Endo *et al.* 2020), aerial and satellite images (ESRI and Google Satellite), and a digital elevation model, all added to the software and observed according to the distribution of features within the area. The main geometric analysis was based on a rose diagram built according to the trend of the traced lines. GeoRose by YongTechnologies software was used to generate a rose diagram of lineament strikes. Every petal corresponds to an interval of 5°, starting from the north (0°) and concentrating every lineament that ranges from 0° to 5°, and so on. The diagram was also divided into eight concentric circles, each one corresponding to an increase of 3% from the center. Thus, the diagram's external perimeter represents 24% of traced lineaments in the correspondent direction.

Preparation of a geotechnical map by multicriteria analysis

The construction of the conceptual geotechnical model consisted of the use of multicriteria analysis methods through cartographic algebra and raster operations that relate parameters and return multiple classification scenarios for the area according to its susceptibility to rupture.

All parameters used were obtained and analyzed remotely, with the help of previous studies (e.g., Vanacôr 2006, Salomão 1999, Reis Jr. and Parizzi 2018). The chosen parameters for the assessment and understanding of the terrain evolution in the study area were:

(i) Slope, indicating zones of greater inclination, in which the requesting forces are intensified by gravity;
(ii) lineament density, representing the level of discontinuity of the rock mass;
(iii) lithotype, defining the strength of the rock material according to its lithological properties.

Table 1. Geotechnical units associated with the study area*.

Geotechnical Unit	Mass movement susceptibility	Dominant Lithology	Geological Unit
1	Low	Granite-gneiss rocks	Belo Horizonte and Caeté complexes
3	Moderate to strong	Itabirites	Itabira Group
4	Very strong	Foliated metamorphic rocks	Caraça and Piracicaba groups
5	Low to moderate	Dolomites	Itabira Group
6	Moderate	Quartzites	Taboões Formation
8	Very strong	Laterites and sediment deposits	-

*The Geotechnical Units described by Reis Jr. and Parizzi (2018) outcrop in the eastern area of our study and the western portion has the same stratigraphic units and rocks. We resort to their classification to define a sequence, from 1 to 5, according to their susceptibility to erosional processes: 1 — low (Unit 1 from Reis Jr. and Parizzi 2018), 2 — low to moderate (Unit 5 from Reis Jr. and Parizzi 2018), 3 — moderate (Unit 6 from Reis Jr. and Parizzi 2018), 4 — moderate to strong (Unit 3 from Reis Jr. and Parizzi 2018), and 5 – very strong (Units 4 and 8 from Reis Jr. and Parizzi 2018).
Source: adapted from Reis Jr. and Parizzi (2018).

The characterization of each variable was made by assigning weights according to their expected influence in each scenario — all visually validated.

Using the v.to.rast tool from the GRASS extension of QGIS, the maps were rasterized into 30 m × 30 m pixels, with predefined values assigned to each classified data element.

A slope raster (Fig. 4) was produced through a 30 m × 30 m pixels resolution SRTM USGS image. Values are presented in percentages, obtained from the ratio of the variation in altitude over the horizontal distance. Thus, 100% represents a 45° slope.

To define the classes in QGIS, the feature *Raster Terrain Analysis (Slope)* was used to obtain the slope in percentage and then the *reclass* function to obtain, initially, the EMBRAPA terrain classification by intervals (EMBRAPA 1979). Every class was suggested and corresponds to a relief class: plane (0–3%), smooth wavy (3–8%), wavy (8–20%), strong wavy (20–45%), and hilly to strong hilly (> 45%). For the EMBRAPA classification, every group aforementioned was given a number from 1 to 5 according to its level of susceptibility to erosional processes, after Salomão (1999) who defines those classes in the very low, low, moderate, strong, and very strong probability of erosional process occurrence. The second form of characterization was conducted according to ungrouped slope percentage values, after Salomão (1999).

The lineaments density map classified the area according to traced lineaments. To this stage, a raster was generated by using the *Line Density* heatmap function (QGIS), which calculates the sum of line vectors inside a circle with a determined area, as mentioned by Oliveira *et al.* (2009). For this study, the input parameters consisted of a search radius of 200 m and pixel dimensions of 30 m. During tests, it was observed that a higher search radius would extrapolate and so increase the influence of lineaments in the analysis, while a lower value would only delimitate the lineaments themselves. Oliveira *et al.* (2009) defined a search area arbitrarily, which corresponds to approximately 300 times smaller than their studied area. Here, we wanted an approach that would consider more of the rock mass compartmentation, so we adopted an area that was about 200 times smaller, but with a search radius corresponding to less than half of the longest lineament traced. Since rock mass resistance depends on its compartmentation and the number of discontinuities, zones with higher lineament densities were considered to be more susceptible to rupture when compared to others.

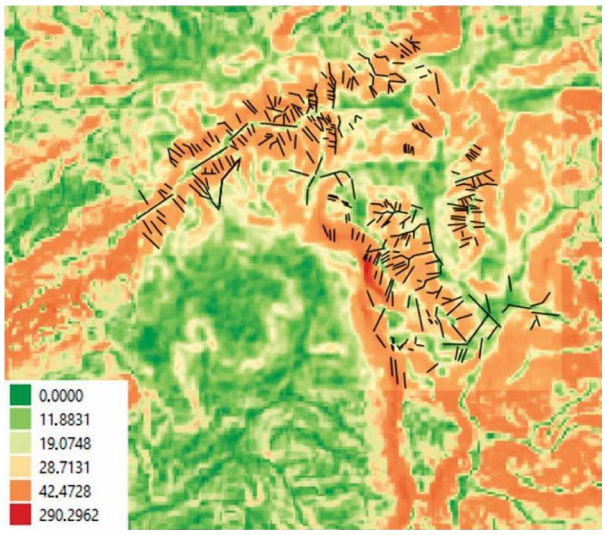

Figure 4. Slope raster with 30 m pixel resolution. Values are indicated in percentage. Lines in black represent lineaments traced.

Finally, the lithotype parameter was used to characterize the area from the perspective of the peculiarities of geotechnical units according to the criteria defined by Reis Jr. and Parizzi (2018) for the rocks of the eastern portion of the metropolitan region of Belo Horizonte. The adaptation of the units defined by the aforementioned authors led to the selection of units 1, 3, 4, 5, 6, and 8 for the study area, according to regional maps and aerial image interpretation (Table 1).

According to Reis Jr. and Parizzi (2018), the granitic-gneissic rocks of geotechnical unit 1, although showing an intense degree of turnover, they are isotropic and homogeneous, with high mechanical strength when unaltered. Therefore, for this study, its susceptibility to rupture was considered low.

Unit 3 (Reis Jr. and Parizzi 2018) is formed by resistant itabirites, but which often develop mass movements with causes associated with the orientation of the slopes, the level of discontinuity, and the degree of alteration of the rock material. In this study, these rocks were classified as having moderate to strong susceptibility to the occurrence of mass movement.

The foliated metamorphic rocks from unit 4 of Reis Jr. and Parizzi (2018) are strongly affected by recurrent discontinuities, which, added to the low mechanical strength of the material, favor the common occurrence of mass movements and block falls due to the displacement of the mass. For this reason, this study considered these rocks to be highly susceptible to mass movements.

Unit 5 dolomites (Reis Jr. and Parizzi 2018) have high mechanical strength and are easily weathered, forming karst features. Rock slides are not common and therefore susceptibility to rupture was here classified as low to moderate.

Geotechnical unit 6 (Reis Jr. and Parizzi 2018) is characterized by quartzites with high mechanical resistance and little susceptibility to weathering. However, in the eastern region of the study area, Reis Jr. and Parizzi (2018) indicate the occurrence of mass movements associated with foliation planes. For this unit, the susceptibility to mass movements was considered moderate.

Geotechnical unit 8 comprises lateritic covers and sediment deposits (alluvium and colluvium), and it is characterized as being highly susceptible to erosion and mass movements, caused by the non-compaction of the sediments and the plasticity associated with clay components. The present work classifies the rocks of this unit as being strongly susceptible to the occurrence of mass movements.

The abovementioned Endo *et al.* (2019) geological units shapefile was rasterized considering the aforementioned classification and a resolution of a 30 m pixel grid. The resulting raster of the lithotype map received grades varying qualitatively between units less likely to have mass movements and units with frequent mass movements.

The three maps resulting from this process present data indicative of zones with a greater and lesser probability of mass movements, according to the parameter used to generate them. However, to establish a correct relationship between them, it was necessary to have a common scale to avoid distortions in the final result. For this, the values that were assigned to the variables of each parameter were all normalized from 0 to 1 by the Equation 1 (Vaz 2019):

$$x' = \frac{x - min\ (x)}{(x)\ - min\ (x)} \qquad (1)$$

Where:
x' = the normalized value;
x = the value to be normalized;
(x) = the dataset.

Finally, using the Raster Calculator tool in QGIS, weighted averages were calculated in order to relate the three maps mathematically. By varying the weights attributed to each parameter, multiple scenarios were constructed to classify the area as to its susceptibility to rupture through changes in slope, lithotype, and lineament density.

LINEAMENT INTERPRETATIONS

It is important to note that photolineaments can be strongly related to geological structures, such as ridges, faults, and regional folds, based on their repetitive geometry, spatial distribution, and association with the directions of the aforementioned structures. The interpretation of lineaments, mapped from aerial photos or other imagery, can be attached to fracture patterns on folds widely known and mapped by several previous works (e.g., Lobato *et al.* 2005, Endo *et al.* 2020). Folds are extremely common deformation structures in any regional terranes. Their geometric features and occurrence bear valuable information on the strain, kinematics, and rheology (Nabavi and Fossen 2021). As for deformation in general, it can be analyzed in terms of geometry (e.g., structural orientation, attitude, size, and morphology or shape), kinematics (involving position, displacement, velocity, and acceleration of as many points as possible and thus progressive deformation), and dynamics (the relationship between forces or stress and kinematics; Yang *et al.* 2019, Nabavi and Fossen 2021). The analysis of fold structures as observed from remote sensing data forms the foundation for understanding and quantifying fold-related deformation.

Two great regional structures will be considered together, and the main function of this research is the application of the technique. Therefore, we will consider the Curral homocline and the Moeda syncline (Fig. 3) as sources of study and not as individual regional structures. Based on the rose diagram analysis (Fig. 5), it was decided to divide the lineaments into four sets: one, varying from 10° to 80°, the second, 80° to 120°, the third, 120° to 160°, and the fourth, 160° to 190°.

The first lineament set (10° to 80°), represented by a green color (Fig. 5), occurs mainly in the northwest and southeast areas. Their estimated lengths vary from 21 to 493 m with an average value of 136 m and a median of 106 m. The second group (80° to 120°), represented by purple (Fig. 5), is well observed in the north and south, with a greater density in the latter. Its minimum value is 38 m, and its maximum is 412 m, with an average of 108 m and a median of 87 m. The third set, represented by a pink color (Fig. 5) (120° to 160°) is concentrated in the northern area, along the ridge. It varies from 21 to 518 m, with an average value of 111 m and a median of 101 m. The fourth group (160° to 190°), represented in blue (Fig. 5), is distributed along the eastern areas from south to north. Their estimated lengths vary from 20 to 390 m with an average value of 119 m and a median of 101 m.

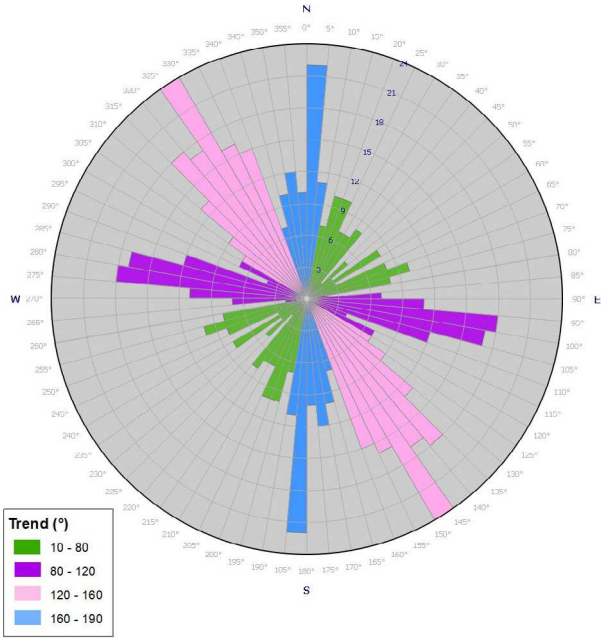

Figure 5. Rose diagram to the analyzed area, separated by the intervals previously defined.

The sets resulting from the grouping of directions of the traced lines are distributed in all units of the Minas Supergroup outcropping in the study area. However, it is possible to identify patterns that relate the lithology to a preferred trend of lines. In this respect, the Cauê Formation encompasses the largest number of guidelines, especially those with a trend between 120º and 160º (Figs. 6 and 7). The lines in this unit are essentially concentrated in the northwestern portion of the area. The Batatal Formation, in turn, has lines with the main direction between 10º and 80º and the Moeda Formation between 80º and 120º — both in the southeast region. The Nova Lima Group, a little outcropping in the area, presented lineaments between 10º and 120º and between 160º and 190º. The Bonfim Complex, the lower limit of the study area, did not present expressive guidelines.

MASS MOVEMENTS CHARACTERIZATION USING SATELLITE IMAGES GEOTECHNICAL INVESTIGATIONS AND MODELING

Several mass movements can be observed, at different scales of movement, in the studied area. The understanding

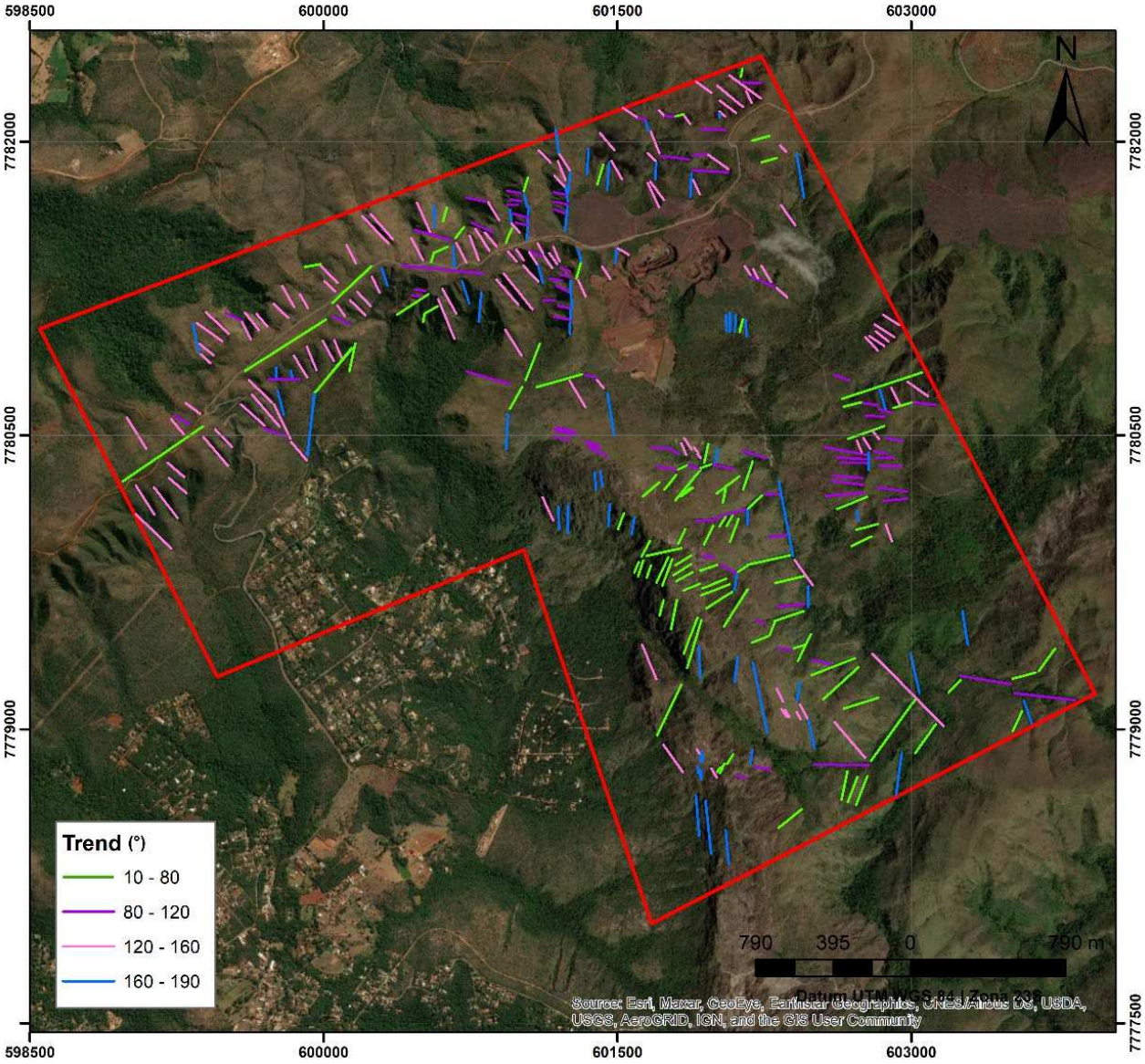

Figure 6. Lineaments traced remotely and divided in sets. Set 1 (10°–80°) in green, Set 2 (80°–120°) in purple, Set 3 (120°–160°) in pink, and Set 4 (160°–190°) in blue. Satellite image from ESRI (2021).

of the phenomenon in this region is imperative to define the nature and the extent of the act, as it can be covered by the extension of Curral Ridge and thus influence the understanding and planning of the surrounding cities.

Geotechnical analysis results

A total of eight scenarios were generated (Fig. 8); the first four (1–4) were classified by using the slope percentage raster without interval reclassification, so its values in the cartographic algebra were not grouped. The last four (5–8) consider the slope percentage classified according to Salomão (1999). Table 2 summarizes the weights given in every scenario.

The map corresponding to scenario 1 was obtained from the attribution of equal weights of 1/3 to each of the three parameters, considering ungrouped values in the slope classification. In this result, the contacts that separate zones of the same susceptibility to mass movements are similar to the lithologic contacts defined by Endo *et al.* (2020; Fig. 9). The greatest probabilities (moderate-to-high and high) occur in the northwest and southeast portions of the study area, with thick patches distributed continuously in these regions. The probability decreases toward the edges of the area, with low-to-moderate or moderate classifications, the former being the most common.

In scenario 2, built with ungrouped values in the slope classification and weights of 0.25 for lithology and lineament density and 0.5 for slope, the map of susceptibility to mass movements presents more homogeneous zones compared to the map of the first scenario. The probabilities in the northwest and southeast areas are essentially classified as moderate-to-high, with narrow patches unexpressive in these stretches — sometimes isolated, as in the northern region. Toward the edges, the predominant probability is low to moderate.

Scenario 3 was generated by matching lithology weighing 0.5, line density 0.2, and slope without EMBRAPA classification 0.3. It is observed that the moderate to highest probabilities are quite hitched with geological units, which are reported to be more susceptible to mass movements, such as metamorphic foliated rocks (e.g., phyllites), itabirites and unconsolidated sediments, and recent sedimentary or lateritic

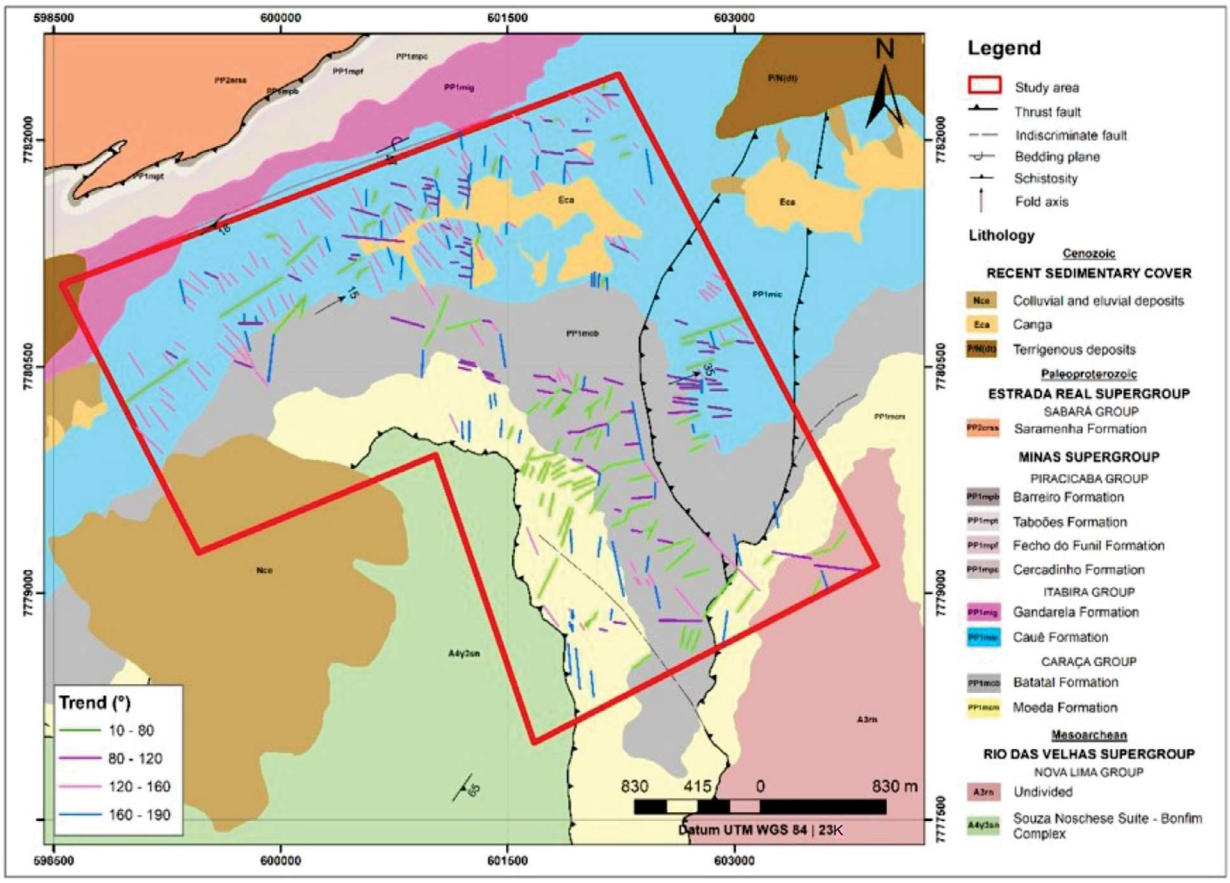

Source: after Endo *et al.* (2019).

Figure 7. Lineament sets vs. Regional Geological Map.

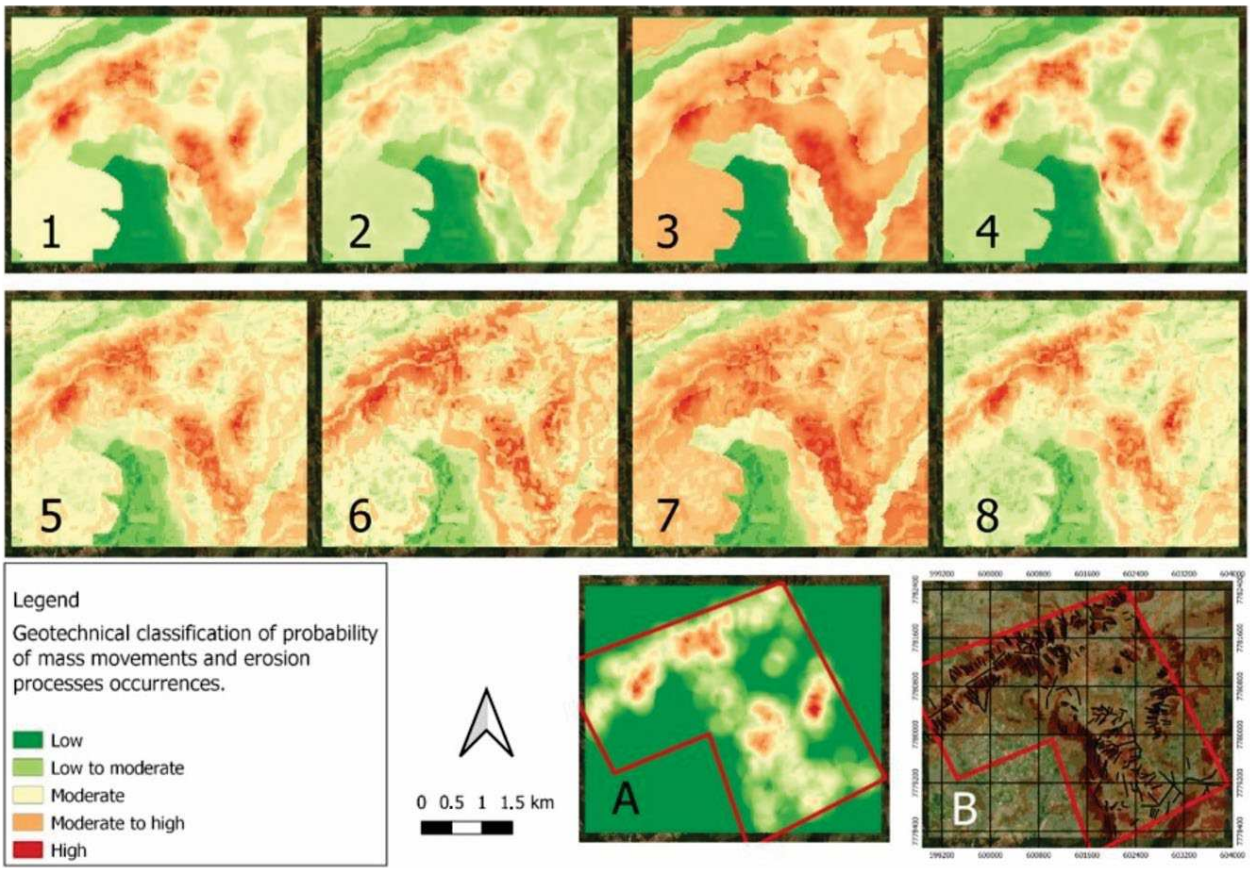

Figure 8. Scenarios of geotechnical analysis based on slope, lithology, and lineament density. Numbers 1–8 correspond to the eight scenarios generated. Map A: line density map where red represents the highest line density values and green the lowest, while yellow are the moderate density areas. Map B represents slope together with traced lineaments (in black), where red is the highest slope and green the lowest.

covers, regardless regions with high slope or high line densities. This way, only dolomite, granitic-gneiss and quartzite terrains are associated with low probability values in the central-south and northwest. It is important to mention that in quartzite cases, exceptions are observed where the slope assumes high values.

When it comes to scenario 4, lithology received a 0.2 weight score, while the other two parameters had the same grade of 0.4. In this case, the observed patterns are remarkably similar to those observed in scenario 2, with moderate-to-high values occurring in the northwest and southeast areas along ridge stretches while low-to-moderate occur toward edges.

The map corresponding to scenario 5 was obtained from the attribution of equal weights to each of the three parameters — as in scenario 1, but considering grouped values in the slope classification (EMBRAPA 1979). Contacts that separate zones with the same susceptibility to mass movements are similar to the lithological contacts defined by Endo *et al.* (2020), with the highest probabilities concentrated in the northwest and southeast portions of the study area (moderate-to-high and high). Heterogeneously, the odds are reduced toward the edges, although isolated spots of moderate-to-high and high probability are common throughout the eastern portion.

For scenario 6, the assigned weights were 0.25 for lithology and lineament density and 0.5 for slope — as in scenario 2 but considering grouped values in the slope classification (EMBRAPA 1979). The greatest probabilities are in the northwest and east portions of the study area (moderate-to-high and high), with homogeneous variations and unclear contacts toward the northeast edge. In general, there is a predominance of moderate-to-high probability zones.

Scenario 7 was obtained by using the same weights as scenario 3, but slope values were grouped according to EMBRAPA (1979). It is observed that geological lithologies strongly control high and low probability domains. Once phyllite, itabirites and recent covers or sedimentary deposits receive a high probability trend while dolomite and gneiss are low-graded.

It is possible to observe that in Scenario 8, with slope classified according to EMBRAPA (1979) and the same weights as Scenario 4, it is possible to observe high values in the northwest to the southeast middle portion, following ridge trends and being accentuated in the high line density and slope regions. Out of these domains, mainly in the extreme northwest and southwest, moderate-to-low probabilities are observed.

Table 2. Weights attributed to parameters used to different scenarios of geotechnical analysis.

Scenario/ Weights	Lithology	Lineament density	Slope
1	1/3	1/3	1/3
2	0.25	0.25	0.5
3	0.5	0.2	0.3
4	0.2	0.4	0.4
5	1/3	1/3	1/3
6	0.25	0.25	0.5
7	0.5	0.2	0.3
8	0.2	0.4	0.4

DISCUSSION AND CONCLUSIONS

The several fracture sets found at the connection between the Curral homocline and Moeda syncline provide qualitative constraints for the temporal and spatial evolution of deformation of the geological layers within the region of focus. The following discussion synthesizes remote sensing observations and published data to make inferences about fold kinematics and geotechnical investigations.

Lineaments and regional structures

The Moeda syncline is the result of Curral nappe's normal limb refolding (Endo *et al.* 2020). In general terms, it is an asymmetric fold with a regional scale and verging for W-SW (Mourão 2007). The Curral anticline materializes the hinge area of the Curral nappe, an allochthonous recumbent megafold represented by the joint of the Serra do Curral and the Moeda syncline. The anticline's axial plane is oriented following 120/30 (Endo *et al.* 2020) and its inverted flap (Oliveira 2005) constitutes the Curral homocline, northwest of the study area.

The group of structures defined by set 1 (green) is distributed in the study area, especially within the Moeda syncline. Its occurrence in the rocks of the Moeda Formation shows

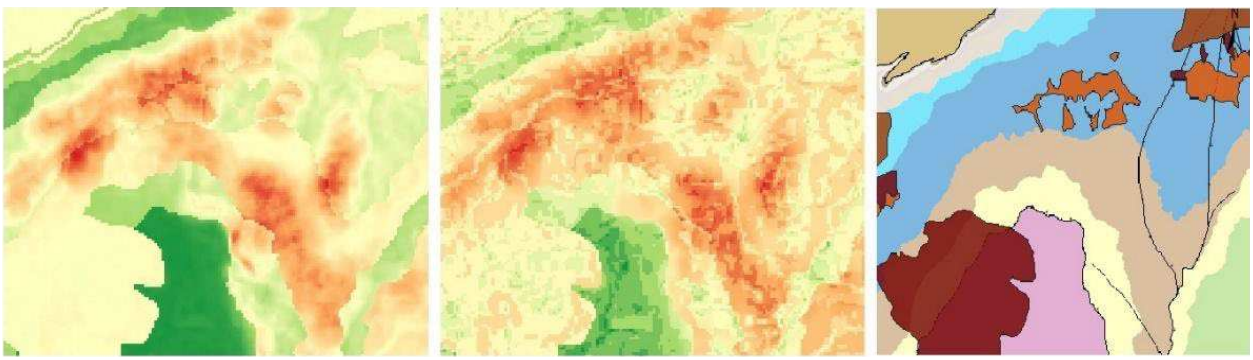

Figure 9. Contacts in the maps of susceptibility to mass movement and erosion of scenarios (A) 1 and (B) 5 and lithological contacts according to Endo *et al.* (2019).

areas where the quartzite bedding planes may intercept the topography. This suggestion is motivated by the orientation pattern of the Curral Ridge bedding planes, which dip toward NW (Fig. 5).

The regional nappes materialized an intersection lineation between the main schistosity and the bedding with an approximate orientation of 095/45 (Fig. 10), and it is parallel to the mineral lineation and the fold axes (Endo and Machado 1997, Almeida *et al.* 2005, Angeli 2015, Rossi and Endo 2015, Barbosa 2018, Endo *et al.* 2019). This pattern of parallelism is confirmed by the linear structures represented in set 2 (purple), focusing on the Cauê Formation itabirites and the Batatal Formation phyllites. Since the direction of the fold axis belongs to set 2, such lines may be associated with the foliation developed in the hinge zone, which corresponds to the north region of the study area.

According to Endo *et al.* (2020), although there are tectonic models that justify this parallelism by shear deformation, such as Cobbold and Quinquis (1980), Ridley (1986), and Sullivan (2013), there are no structures that corroborate this (e.g., sheath folds). Therefore, Endo *et al.* (2020) suggest that the parallelism of linear structures is associated with deformation in a constriction flow regime. In this context, applying the Lin and Jiang (2001) model to lineations in transpressive shear zones, the constriction flow regime may have been developed as a function of the kinematics of the São Vicente Shear Zone, whose curvature guided the lineaments from an accumulation of deformation (Fig. 11).

The grouped lines in set 3 (pink) reverberate in the Cauê Formation, especially within the Curral homocline, and may indicate stretching lineation related to movements between Cauê beds; favorable direction for the occurrence of mafic dykes that are NW-SE oriented, as mentioned by Endo *et al.* (2020); or simply related to the Curral homocline watershed mechanism, since it is a topographic top.

The grouped lines in set 4 (blue) are distributed across all outcropping lithologies in the study area. Suggestions of features that justify the orientation of these guidelines based on the observed frequency and the specific context of the junction of the Moeda syncline with the Curral homocline were not found in the geological historical data.

Large folds can influence landscape evolution during erosion, typically with ridges along with steep limbs and valleys along synforms, or with resistant cores creating positive topographic landforms. Folds and folding furthermore influence the evolution of the Earth's surface as they form, controlling patterns of erosion, sediment routing and depocenters. These processes cause rapid stratigraphic thickness variations that relate to the growth history of the folds (Nabavi and Fossen 2021).

As a great approximation, the lineaments analyses from the connection between Curral homocline and Moeda syncline presented here in suggest having azimuth direction compatibility with the more known, previously published studies in the area.

Landslide characterization using satellite images geotechnical investigations and modelling

As discussed by Lageson *et al.* (2012), the scope of this project was to apply Google Earth Pro and remote sense data for the collection and preliminary interpretation of orientation data of lineaments and their future use. As the example here, we propose the geotechnical investigations, based on the images collected in Google Earth Pro, as well as from the other databases aforementioned. With the present purpose, we aim to understand and apply techniques that combine geometric, geological, and geomorphological data.

A systematic and comparative analysis of the eight maps of susceptibility to mass movement and erosion was conducted to qualify the results obtained by using each weight distribution in the multi-criteria analysis. The qualification of the scenarios and their respective methods was conducted by observing the weights attributed to parameters more or less relevant to stability (between slope, lineament density, and lithology), analyzed in general for rock masses and specifically in the context of the area of this study.

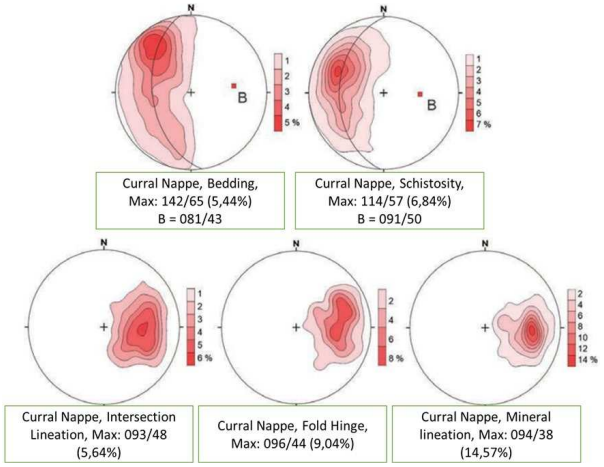

Source: modified from Endo *et al.* (2020).

Figure 10. Curral Nappe's structures orientation represented in stereographic projections. Top-left and top-right images represent bedding (S0) and schistosity (Sn), respectively. Bottom images, from left to right, intersection lineation, fold hinge, and mineral lineation.

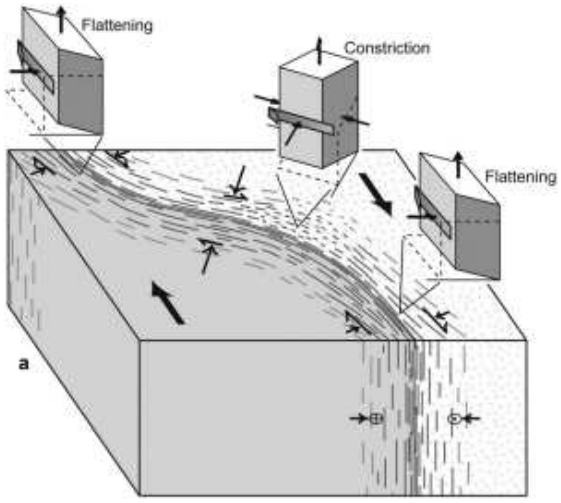

Source: modified from Sullivan (2013).

Figure 11. Conceptual model representing the arrangement of linear structures in curved portions of shear zones.

In all results, the highest probability of the occurrence of mass movements and erosion corresponds to the alignments of the ranges in the SW-NE and NW-SE directions. The main associated lithotypes belong to the Batatal and Cauê formations, and it is in these areas where the highest lineament densities and steepest slopes are found. The eight maps show a pattern of probability reduction toward the edges of the area, where the relief is smoother and there is a lower density of lineaments. In these zones, the predominant lithotype corresponds to the Cauê Formation.

Scenarios 1 and 5 were both the results of calculations with equal weights for the 3 parameters (Figs. 8 and 9); however, in scenario 5, the slope values were grouped into intervals, whereas in scenario 1, these values are continuous. In both scenarios, the similarity between susceptibility map contacts and lithologic map contacts (Fig. 9) reflects a low contribution of slope and lineament density to definitions of susceptibility to mass movements. Since the standard of discontinuity of the material and the slope of the terrain are factors of great relevance to the instability of rock masses (Bigarella 2003, Pradhan *et al*. 2006, Pinto *et al*. 2013, Fiori 2016), it may be inconsistent that the limits between rocks of the same strength stand out on maps of susceptibility to mass movement.

The greater reach of higher probability zones in scenario 5 compared to scenario 1, especially near the edges (Figs. 8 and 9), may be associated with areas of smoother relief in which slope was more relevant when the values were grouped, as they now occupy positions equivalent to steeper slopes. This variation in data usage increased the spread of moderate-to-high susceptibility zones.

Scenarios 2 and 6 (Fig. 8), although both are the result of calculations made with weights of 0.25 for lithotype and lineament density and 0.5 for slope, suffered the greatest variations due to the grouping of slope values since this parameter was the most influential in the multi-criteria analysis. Several authors (Pradel *et al*. 1993, Bigarella 2003, Pradhan *et al*. 2006, Pinto *et al*. 2013) demonstrate the importance of slope in rock mass stability research.

Great differences are not observed when scenarios 3 and 7 are compared (Fig. 8). Generally, the domains of high or low values are maintained, except for regions where quartzites refer to the geological unities. In these cases, when scenario 3 presents quartzite regions as low-to-moderate probability, scenario 7 exhibits them as moderate, with high slope places demarking moderate-to-high probability. Both the scenarios show that lithology units scored 5 on the respective scale, demonstrating at least a moderate-to-high probability, even when slope values are very low and there is no lineament traced.

When ungrouped, the slope values considerably reduced the occupation of zones with some probability of developing mass movements — zones of moderate-to-high susceptibility — were essentially concentrated in the alignment of the ranges, where the greatest slopes and the greatest density of lineaments are found. The grouped values resulted in large areas of high susceptibility in the Batatal and Cauê formations outcropping in the eastern portion, due to the inclusion of intermediate slopes in high slope groups. This phenomenon can be well observed in Scenarios 4 and 8; in the former, high values are mostly attached to ridges, where the slope is elevated and there is a higher number of lineaments, and these regions are surrounded by a thin area characterized by its moderate values. When it comes to Scenario 8 (Fig. 8), high values in ridge-attached regions assume a larger area, and thin moderate regions get vaster. In a comparative analysis between the scenarios obtained and the aerial image of the GEP, it was observed that some areas of slopes classified as susceptible in scenarios 4 and 8 have transported material in their bases, probably from mass movements or erosional processes that occurred previously (Fig. 12).

Finally, another Google Earth Pro application proved to be exceptionally useful in the analysis of geotechnical investigations where areas of greater and lesser probability of mass movements and erosion are possible to indicate. Experience has shown that we also had difficulty "seeing" a down-plunge view on a 2D map (as did the students of Lageson *et al*. 2012).

The COVID-19 pandemic and the serious Brazilian institutional crisis challenged researchers and managers to find palliative measures that would prevent the collapse of scientific research and practical work in geosciences in recent years. Based on the aforementioned works, this application proposal sought to systematize the use of existing data produced by remote sensors, aiming to minimize the impacts of social distancing measures in the COVID-19 epidemic, which prevented field trips from being carried out in Brazil, from 2020 to 2021. It is also important to think about how society has changed and adapted in the post-pandemic period. We need to think about a world that combines remote work and face-to-face work, in pandemic and non-pandemic situations.

The use of lineament density, lithotype, and slope parameters to develop rupture susceptibility research was effective for this work, considering the possibility of being analyzed using remote sensing techniques as well as its great relevance in previous studies focused on this theme (e.g., Cruz 1974, Pradel *et al*. 1993, Bigarella 2003, Pradhan *et al*. 2006, Schaefer *et al*. 2012).

As clearly explained by Nabavi and Fossen (2021), folds and folding furthermore influence the evolution of the Earth's surface as they form, controlling patterns of erosion, sediment routing, and depocenters. These authors also discuss how these points are particularly relevant to mining operations and the prediction of ore bodies at depth. Fold structures can also control the stability and behavior of natural and engineered rock slopes depending on their orientations, geometry, and structural complexity concerning a given slope face.

In an area with well-defined structural patterns, it is possible to remotely identify lineaments and fractures and associate them with already mapped regional structures. In this case, the less common lineaments observed, which are trending in the northeast direction, are probably related to the Moeda Formation bedding strike. Lineaments tending east are possibly related to mineral lineation, fold axes, and dip direction, and they occur mainly in the Batatal and Cauê Formations. Southeast lineaments could be associated with both interstrata stretching lineaments and preferential directions of

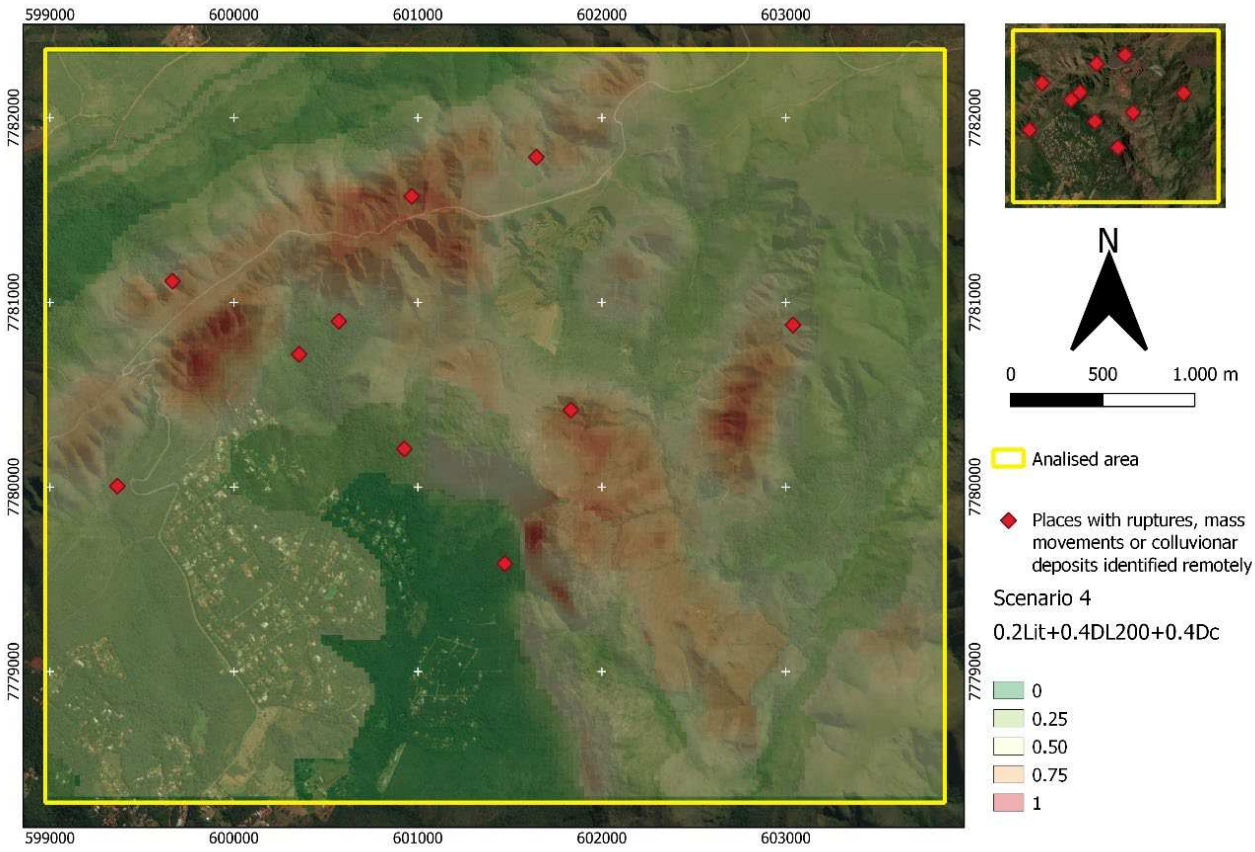

Figure 12. Areas of slopes transported material in their basis, probably from mass movements, identified remotely. Background is represented by scenario 4.

mafic dykes reported in the area. However, this group of lineaments could simply be related to the Curral ridge watershed mechanism, since their direction is perpendicular to the ridge extension. More detailed information should be investigated to obtain more accurate interpretations of the southeast and NS lineament directions.

The systematic and comparative analysis of the final scenarios obtained by varying the weights attributed to each parameter highlighted the importance of observing the lineaments identified in aerial images, as they may represent local discontinuities and regional structures capable of compromising the stability of the mass. The nature of these guidelines and their relationship with the sloping plane must be affirmed in the field so that their degree of interference is fully understood. Similarly, it was observed that a coherent assessment of influences requires that the slope of the ramp also have representative participation, with equal or similar weight to the weight of the lineaments' density. The minor influence of lithology type can be inferred by evaluating Bieniawski (1989) RMR classification. In their analysis, the rock type itself is parameterized according to its uniaxial compressive strength, which relates to internal friction angle and cohesion (Labuz and Zang 2012), characteristics that are inherent to the rock. On the contrary, discontinuities-related parameters appear in the RMR more than once (RQD — rock quality designation, spacing, and conditions of discontinuities). This way, it is possible to deduce that density lineaments, which have to do with the compartmentation of the rock mass, influence rupture processes more than the lithotype. Since kinematic analysis depends on internal friction angle, resistance, and requesting stress (Hoek and Bray 1989), and the first two are rock parameters that change in a strongly defined interval depending on rock conditions, slope level directly influences requesting forces, since this ramp feature can control how block weight is distributed between shearing and normal stress in a rupture plane. Its analysis is more rational when its values are ungrouped so that intermediate slopes are not included in very low or very high slope groups. Taking into account the greater relevance of these two parameters (concerning the lithotype) is a strategy used in several relevant works on slope stability (e.g., Cruz 1974, Bigarella 2003, Pradhan *et al*. 2006, Schaefer *et al*. 2012, Pinto *et al.* 2013). From this perspective, the best scenario resulting from the processes included in this study was scenario 4, which assigned weights of 0.4 for lineament density and slope (in ungrouped values) and 0.2 for the lithotype. Through comparative visual validation between the map of scenario 4 and the aerial image of Google Earth, this choice is also suggested by the observation of unconsolidated material on slopes classified as more susceptible. However, if one desires to run a more conservative analysis, one should choose scenario 8 once its higher value domains are expanded since intermediate slopes (above 20%) are assigned to higher probabilities.

Based on the methods adopted in this study, choosing the best scenario that characterizes an area in terms of susceptibility to the occurrence of rupture must include specific considerations for the context analyzed, such as regional patterns

that affect the relevance of the parameters. In addition, the study must establish the grade of conservatism to be adopted, especially for slope classifications. Using slope values grouped into intervals, for example, leads to less detailed results about intermediate slopes, contributing to a less conservative final analysis than that made with ungrouped slopes. The level of conservatism suitable for each study must consider several factors, such as urban occupation, rainfall, and the frequency of mass movements in the region.

Geometrical analysis and classification form the foundation for the use of folds in structural/tectonic analysis. In general, understanding fold geometries, folding mechanism, strain history, as well as relationships in fracture networks are critical for the prediction of the structural style and variations, and important in a wide range of applications, including fractured reservoir exploration, carbon capture, and storage, aquifer characterization, civil engineering, mining industry, and seismic hazard prediction (following Nabavi and Fossen 2021).

ACKNOWLEDGMENTS

This research is the result of the completion of course work by the students at the Universidade Federal de Minas Gerais-UFMG, defended in 2022. It was an adapted idea due to the impossibility of classic field mapping due to the outbreak of COVID-19 pandemic. We thank Fabrício Lisboa for sharing some insights that were extremely important to this methodology development and analysis, and for helping with QGIS, and Franco Naghetini for some ideas that helped in the validation of obtained results. We also thank the publication that provided the original idea and its authors (Lageson *et al.* 2012). We are also grateful for the great contributions made by the anonymous reviewers.

ARTICLE INFORMATION

Manuscript ID: 20220040. Received on: 30 OCT 2021. Approved on: 16 MAY 2022.

How to cite this article: Roncato J., Martins M.M., Silva M.M.L. 2023. Remote sensing applied to geological, structural, and mass movements characterization in the connection between Curral Homocline and Moeda Syncline, Quadrilátero Ferrífero Region, Brazil. *Brazilian Journal of Geology*, **53**(1): e20220040. https://doi.org/10.1590/2317-4889202320220040

J.R.: Conceptualization, Data curation, Formal Analysis, Investigation, Methodology, Project administration, Resources, Software, Supervision, Validation, Visualization, Writing — original draft, Writing — review & editing. M.M.M.: Conceptualization, Data curation, Investigation, Methodology, Software, Validation, Visualization, Writing — original draft. M.M.L.S.: Conceptualization, Data curation, Investigation, Methodology, Software, Validation, Visualization, Writing — original draft.

Competing interest: the authors declare no competing interests.

REFERENCES

Alkmim F.F., Marshak S. 1998. Transamazonian orogeny in the Southern Sao Francisco craton region, Minas Gerais, Brazil: evidence for Paleoproterozoic collision and collapse in the Quadrilátero Ferrıfero. *Precambrian Research*, **90**(1-2):29-58. https://doi.org/10.1016/S0301-9268(98)00032-1

Almeida F.F.M. de, Hasui Y., Brito Neves B.B. de. 1976. The upper precambrian of South America. *Boletim IG*, **7**:45-80.

Almeida L.G., Castro P.T.A., Endo I., Fonseca M.A. 2005. O Grupo Sabará no Sinclinal Dom Bosco, Quadrilátero Ferrífero: uma revisão estratigráfica. *Brazilian Journal of Geology*, **35**(2):177-186.

Angeli G. 2015. *Arcabouço estrutural e contribuição à estratigrafia do Grupo Maquiné, Quadrilátero Ferrífero, Minas Gerais*. Dissertação de Mestrado, Departamento de Geologia da Universidade Federal de Ouro Preto, Ouro Preto.

Baltazar O.F., Zucchetti M. 2007. Lithofacies associations and structural evolution of the Archean Rio das Velhas greenstone belt, Quadrilátero Ferrífero, Brazil: A review of the setting of gold deposits. *Ore Geology Reviews*, **32**(3-4):471-499. https://doi.org/10.1016/j.oregeorev.2005.03.021

Barbosa L.H. do C. 2018. Serra do Itacolomi revisitada: estratigrafia, arcabouço estrutural e aplicação de métodos geofísicos. Monografia (Graduação em Engenharia Geológica), Escola de Minas, Universidade Federal de Ouro Preto, Ouro Preto.

Bellahsen N., Fiore P., Pollard D.D. 2006. The role of fractures in the structural interpretation of Sheep Mountain Anticline, Wyoming. *Journal of Structural Geology*, **28**(5):850-867. https://doi.org/10.1016/j.jsg.2006.01.013

Bieniawski Z.T. 1989. *Engineering rock mass classifications:* a complete manual for engineers and geologists in mining, civil, and petroleum engineering. John Wiley & Sons.

Bigarella J.J. 2003. *Estrutura e origem das paisagens tropicais e subtropicais*. Florianópolis: Ed. da UFSC, v. 3.

Carneiro M.A. 1992. *O complexo metamórfico Bonfim setentrional: evolução geológica de um segmento arqueano de crosta continental*. Unpublished PhD thesis, Universidade de São Paulo, Instituto de Geociências, São Paulo.

Christofoletti A. 1999. *Modelagem de sistemas ambientais*. São Paulo: Edgard Blücher.

Cobbold P.R., Quinquis H. 1980. Development of sheath folds in shear regimes. *Journal of Structural Geology*, **2**(1-2):119-126. https://doi.org/10.1016/0191-8141(80)90041-3

Cordani U.G., Kawashita K., Mueller G., Quade H., Reimer V., Roeser H. 1980. Tectonic-and petrological interpretation of geochronological data on the basement at the Southeast border of the Quadrilátero Ferrífero, Minas Gerais, Brazil. *Anais da Academia Brasileira de Ciências*, **52**(4):785-799.

Costa M.F. da, Kyle J.R., Lobato L.M., Ketcham R.A., Figueiredo e Silva R.C., Fernandes R.C. 2022. Orogenic gold ores in three-dimensions: a case study of distinct mineralization styles at the world-class Cuiabá Deposit, Brazil, using high-resolution X-ray computed tomography on gold particles. *Ore Geology Reviews*, **140**:104584. https://doi.org/10.1016/j.oregeorev.2021.104584

Cruz O. 1974. *A serra do Mar e o litoral na área de Caraguatatuba, SP:* contribuição à geomorfologia litorânea tropical. Teses e Monografias. São Paulo: Universidade de São Paulo, 181 p.

Dorr J.V.N. 1969. *Physiographic, stratigraphic, and structural development of the Quadrilatero Ferrifero, Minas Gerais, Brazil*. U.S. Government Printing Office.

Dorr J.V.N., Gair J.E., Pomerone J.B., Rynearson G.A. 1957. *Revisão Estratigráfica Pré-Cambriana do Quadrilátero Ferrífero*. Rio de Janeiro: DNPM/DFPM. 36 p. (Avulso 81).

Dorr II J.V.N., Gair J.E., Pomerene J.G., Rynearson G.A. 1957. *Revisão da estratigrafia précambriana do Quadrilátero Ferrífero*. Brasília: Divisão de Fomento da Produção Mineral. v. 81.

Dutra L.F. 2017. *Caracterização geocronológica U-Th-Pb de zircões detríticos na porção nordeste do sinclinal Gandarela-implicações para evolução sedimentar e geotectônica do Quadrilátero Ferrífero*. Dissertation, Universidade Federal de Ouro Preto, Ouro Preto.

EMBRAPA - Empresa Brasileira de Pesquisa Agropecuária. 1979. *Serviço Nacional de Levantamento e Conservação de Solos*. Súmula das 10. Reunião Técnica de Levantamento de Solos. Rio de Janeiro: EMBRAPA, 83 p. (EMBRAPASNLCS. Micelânea, 1.)

Endo I., Galbia H.F., Delgado C.E.R., Oliveira M.M.F., Zaparolli A. de C., Moura L.G.B. de, Peres G.G., Oliveira A.H. de, Zavaglia G., Danderfer F.A., Gomes C.J.S., Carneiro M.A., Nalini Jr. H.A., Castro P. de T.A., Suita M.T. de F., Seixas L.A.R., Tavaza E., Lana C. de C., Marns-Neto M.A., Marns M. de S., Ferreira F.F.A., Franco A.P., Almeida L.G., Rossi D.Q., Angeli G., Madeira T.J.A., Piassa L.R.A, Mariano D.F., Mariano D.F., Carlos D.U. 2019. *Mapa geológico do Quadrilátero Ferrífero, Minas Gerais, Brasil*. Escala 1:50.000. Ouro Preto: Departamento de Geologia, Escola de Minas, UFOP, Centro de Estudos Avançados do Quadrilátero Ferrífero.

Endo I., Machado R. 1997. Regimes tectônicos no segmento meridional do Cráton do São Francisco: região do Quadrilátero Ferrífero, Minas Gerais. In: Simpósio de Geologia de Minas Gerais, 9., 1997, Ouro Preto. Anais, Boletim 14:58-59. Ouro Preto: SBG Núcleo MG.

Endo I., Delgado C.E.R., Oliveira M.M.F., Zapparoli A.C., Carlos D.U., Galbiatti H.F., Castro P.T.A., Suita M.T.F., Barbosa M.S.C., Lana C.E., Moura L.G.B. 2019. *Estratigrafia e Arcabouço Estrutural do Quadrilátero Ferrífero:* Nota Explicativa do Mapa Geológico do Quadrilátero Ferrífero, Minas Gerais, Brasil. Escala 1:150.000. Ouro Preto: Departamento de Geologia da Escola de Minas, Centro de Estudos Avançados do Quadrilátero Ferrífero.

Endo I., Machado R., Galbiatti H.F., Rossi D.Q., Zapparoli A.C., Delgado C.E.R., Castro P.T.A., Oliveira M.M.F. 2020. Estratigrafia e evolução estrutural do Quadrilátero Ferrífero, Minas Gerais. In: Castro P.T.A., Endo I., Gandini A.L. (eds.). *Quadrilátero Ferrífero:* avanços do conhecimento nos últimos 50 anos, v. 50. Belo Horizonte: 3i.

ESRI. 2021. *"World Imagery" [basemap]*. Scale Not Given. "World Imagery". Available at: https://www.arcgis.com/apps/mapviewer/index.html?layers=10df2279f9684e4a9f6a7f08febac2a9. Accessed on: Jun 19, 2021.

Farina F., Albert C., Dopico C.M., Gil A., Moreira H., Hippertt J.P., Cutts K., Alkmim F.F., Lana C. 2016. The Archean–Paleoproterozoic evolution of the Quadrilátero Ferrífero (Brasil): Current models and open questions. *Journal of South American Earth Sciences*, **68**:4-21. https://doi.org/10.1016/j.jsames.2015.10.015

Fiori A.P. 2016. *Fundamentos de mecânica dos solos e das rochas*. São Paulo: Oficina de Textos.

Gair J.E. 1962. *Geology and ore deposits of the Nova Lima and Rio Acima quadrangles, Minas Gerais, Brazil*. U.S. Geology Survey Professional Paper 341-A. U.S. Geology Survey, 67 p.

Hartmann L.A., Leite J.A.D., Silva L.C., Remus M.V.D., McNaughton N.J., Groves D.I., Fletcher I.R., Santos J.O.S., Vasconcellos M.A.Z. 2000. Advances in SHRIMP geochronology and their impact on understanding the tectonic and metallogenic evolution of southern Brazil. *Australian Journal of Earth Sciences*, **47**(5):829-844. https://doi.org/10.1046/j.1440-0952.2000.00815.x

Hedlund C.A., Anastasio D.J., Fisher D.M. 1994. Kinematics of fault-related folding in a duplex, Lost River Range, Idaho, USA. *Journal of Structural Geology*, **16**(4):571-584. https://doi.org/10.1016/0191-8141(94)90098-1

Herz N. 1970. *Gneissic and igneous rocks of the Quadrilátero Ferrífero, Minas Gerais, Brazil:* U.S. Geological Survey Professional Paper. U.S. Geological Survey.

Hoek E., Bray J. 1989. *Rock slopes:* design, excavation, stabilization. UC Berkeley Transportation Library.

Johnson K.M., Johnson A.M. 2002. Mechanical models of trishear-like folds. *Journal of Structural Geology*, **24**(2):277-287. https://doi.org/10.1016/S0191-8141(01)00062-1

Labuz J.F., Zang A. 2012. Mohr–Coulomb failure criterion. In: *The ISRM Suggested Methods for Rock Characterization, Testing and Monitoring: 2007-2014*. Cham: Springer, p. 227-231.

Ladeira E.A. 1991. Genesis of gold in Quadrilatero Ferrifero: a remarkable case of permanency, recycling and inheritance: a tribute to Djalma Guimares, Pierre Routhier and Hans Ramberg. In: Symposium Brazil Gold'91, 1991. *Anais…* p. 11-30.

Lageson D.R., Larsen M.C., Lynn H.B., Treadway W.A. 2012. Applications of Google Earth Pro to fracture and fault studies of Laramide anticlines in the Rocky Mountain foreland. *Geological Society of America Special Papers*, **492**:209-220. https://doi.org/10.1130/2012.2492(15)

Lana C., Alkmim F.F., Armstrong R., Scholz R., Romano R., Nalini Jr. H.A. 2013. The ancestry and magmatic evolution of Archaean TTG rocks of the Quadrilátero Ferrífero province, southeast Brazil. *Precambrian Research*, **231**:157-173. https://doi.org/10.1016/j.precamres.2013.03.008

Lin S., Jiang D. 2001. Using along-strike variation in strain and kinematics to define the movement direction of curved transpressional shear zones: an example from northwestern Superior Province, Manitoba. *Geology*, **29**(9):767-770. https://doi.org/10.1130/0091-7613(2001)029%3C0767:UASVIS%3E2.0.CO;2

Lobato L.M., Baltazar O.F., Reis L.B., Achtschin A.B., Baars F.J., Timbó M.A., Berni G.V., Mendonça B.R.V., Ferreira D.V. 2005. *Projeto Geologia do Quadrilátero Ferrífero-integração e correção cartográfica em SIG com nota explicativa*. Belo Horizonte: CODEMIG, v. 1.

Machado N., Schrank A., Noce C.M., Gauthier G. 1996. Ages of detrital zircon from Archean-Paleoproterozoic sequences: Implications for Greenstone Belt setting and evolution of a Transamazonian foreland basin in Quadrilátero Ferrífero, southeast Brazil. *Earth and Planetary Science Letters*, **141**(1-4):259-276. https://doi.org/10.1016/0012-821X(96)00054-4

Madeira M.R. 2018. *Evolução sedimentar e história deformacional da Formação Moeda ao longo da junção entre o Sinclinal da Moeda e o Homoclinal da Serra do Curral, Quadrilátero Ferrífero, MG*. Dissertação de Mestrado, Universidade Federal de Ouro Preto, Ouro Preto.

Marshak S., Alkmim F.F. 1989. Proterozoic contraction/extension tectonics of the southern São Francisco region, Minas Gerais, Brazil. *Tectonics*, **8**(3):555-571. https://doi.org/10.1029/TC008i003p00555

Medina A.I., Dantas M.E., Saadi A. 2005. *Projeto APA SUL RMBH-Estudos do Meio Físico*. Belo Horizonte: CPRM/SEMAD/CEMIG, v. 6.

Minas Gerais. 2007. *Plano de Manejo do Parque Estadual da Serra do Rola-Moça, incluindo a Estação Ecológica de Fechos*. Encarte 3 – A unidade de conservação. Belo Horizonte: Biodiversitas, 213 p.

Minas Gerais. Instituto Estadual de Florestas. *Parques Estaduais*. Available at: http://www.ief.mg.gov.br/component/content/article/3306-nova-categoria/2836-parques-estaduais. Accessed on: Jun 8, 2020.

Moreira H., Lana C., Nalini Jr. H.A. 2016. The detrital zircon record of an Archaean convergent basin in the Southern São Francisco Craton, Brazil. *Precambrian Research*, **275**:84-99. https://doi.org/10.1016/j.precamres.2015.12.015

Moreira I.C. 1999. *Avaliação das áreas de risco ambientais urbanos do vale do Quitite - Jacarepaguá-RJ*. Monografia, Departamento de Geociências, Universidade Federal Rural do Rio de Janeiro, Rio de Janeiro, 49 p.

Mourão M.A.A. 2007. Caracterização hidrogeológica do aquífero cauê, quadrilátero ferrífero, MG: Subsídios para a gestão dos recursos hídricos no quadrilátero ferrífero. Tese de Doutorado, Universidade Federal de Minas Gerais, Belo Horizonte.

Nabavi S.T., Fossen H. 2021. Fold geometry and folding–a review. *Earth-Science Reviews*, **222**:103812. https://doi.org/10.1016/j.earscirev.2021.103812

National Aeronautics and Space Administration (NASA). 2013. *Shuttle Radar Topography Mission (SRTM) Global*. Distributed by OpenTopography. https://doi.org/10.5069/G9445JDF

Noce C.M. 1995. *Geocronologia dos eventos magmáticos, sedimentares e metamórficos na região do Quadrilátero Ferrífero, Minas Gerais*. Tese de Doutorado, Universidade de São Paulo, São Paulo.

Oliveira D.B., Moreno R.S., Miranda D.J., Silva Ribeiro C.S., Seoane J.C.S., Melo C.L. 2009. Elaboração de um mapa de lineamento estrutural e densidade de lineamento através de imagem SRTM, em uma área ao norte do rio Doce, ES. In: Simpósio Brasileiro de Sensoriamento Remoto, 14., 2009. Anais... p. 4157-4163.

Oliveira L.N. de. 2015. *Análise da suscetibilidade e potencial à erosão laminar no município de São Miguel do Araguaia–GO*.

Oliveira N.V. de. 2005. *Modelagem e inversão 2D de dados magnetométricos aplicados na caracterização da geometria do Sinclinal Gandarela e Homoclinal Curral – Quadrilátero Ferrífero, MG*. Dissertação de Mestrado em Evolução Crustal e Recursos Naturais, Universidade Federal de Ouro Preto, Ouro Preto.

Pereira M.C., Stávale Y.O., Salgado A.A.R. 2013. Estudo da gênese das cavidades e depressões em minério de ferro-Quadrilátero Ferrífero/MG: serras do Rola Moça e do Gandarela. *Revista Brasileira de Geomorfologia*, 13(3):245-253. https://doi.org/10.20502/rbg.v13i3.173

Pinto R.C., Passos E., Caneparo S.C. 2013. Considerações a respeito dos condicionantes utilizados em pesquisas envolvendo movimentos de massa. *Geoingá*, **5**(1):102-124. https://doi.org/10.4025/geoinga.v5i1.49211

Pradel D., Raad G. 1993. Effect of permeability on surficial stability of homogeneous slopes. *Journal of Geotechnical Engineering*, **119**(2):315-332. https://doi.org/10.1061/(ASCE)0733-9410(1993)119:2(315)

Pradhan B., Singh R.P., Buchroithner M.F. 2006. Estimation of stress and its use in evaluation of landslide prone regions using remote sensing data. *Advances in Space Research*, **37**(4):698-709. https://doi.org/10.1016/j.asr.2005.03.137

Reis Jr. W., Parizzi M.G. 2018. Caracterização das unidades geotécnicas da porção leste da região metropolitana de Belo Horizonte–MG. *Geonomos*, **26**(2):23-30. https://doi.org/10.18285/geonomos.v26i2.12565

Renger F.E., Noce C.M., Romano A.W., Machado N. 1994. Evolução sedimentar do Supergrupo Minas: 500 Ma. de registro geológico no Quadrilátero Ferrífero, Minas Gerais, Brasil. *Geonomos*, **2**(1):1-11. https://doi.org/10.18285/geonomos.v2i1.227

Ridley J. 1986. Parallel stretching lineations and fold axes oblique to a shear displacement direction—a model and observations. *Journal of Structural Geology*, **8**(6):647-653. https://doi.org/10.1016/0191-8141(86)90070-2

Romano A.W. 1989. *Évolution tectonique de la région nord-ouest du quadrilatère ferrifère: Minas Gerais-Brésil (Géochronologie du socle, aspects géochimiques et pétrographiques des supergroupes Rio Das Velhas et Minas)*. Tese de Doutorado, Nancy 1.

Romano R., Lana C., Alkmim F.F., Stevens G.S., Armstrong R. 2013. Stabilization of the southern portion of the São Francisco Craton, SE Brazil, through a long-livedperiod of potassic magmatism. *Precambrian Research*, **224**:143-159. https://doi.org/10.1016/j.precamres.2012.09.002

Roncato J.G. 2016. *Evolução de turbiditos e sua mineralização aurífera no lineamento Córrego do Sítio e área Cuiabá-Lamego, Supergrupo Rio das Velhas: Geoquímica, Geocronologia in situ LA-ICP-MS em sulfetos*. Tese de Doutorado, Universidade Federal de Minas Gerais, Belo Horizonte, 301 p.

Roncato J.G., Almeida A.L.C., Macedo B., Oliveira M. 2020. Análise geofísica da região do Rio Conceição, Quadrilátero Ferrífero, associados a dados de campo, petrográficos e de imagens aéreas. *Geosciences = Geociências*, **39**(1):47-63. https://doi.org/10.5016/geociencias.v39i1.14613

Roncato J.G., Lobato L.M., Lima L.C., Porto C.G., Silva R.C.F. 2015. Metaturbidite-hosted gold deposits, Córrego do Sítio lineament, Quadrilátero Ferrífero, Brazil. *Brazilian Journal of Geology*, **45**(1):5-22. https://doi.org/10.1590/23174889201500010001

Rosi A., Vannocci P., Tofani V., Gigli G., Casagli N. 2013. Landslide Characterization Using Satellite Interferometry (PSI), Geotechnical Investigations and Numerical Modelling: The Case Study of Ricasoli Village (Italy). *International Journal of Geosciences*, **4**(5):904-918. https://doi.org/10.4236/ijg.2013.45085

Rosière C.A., Spier C.A., Rios F.J., Suckau V.E. 2008. The Itabirite from the Quadrilátero Ferrífero and related high-grade ores: a review. *Reviews in Economic Geology*, **15**:223-243. https://doi.org/10.5382/Rev.15.09

Rossi D.Q., Endo I. 2015. A structural model of the Fábrica Nova region, Santa Rita syncline, Quadrilátero Ferrífero: flanking folds as a folding mechanism. *REM: Revista Escola de Minas*, **68**(2):153-162. https://doi.org/10.1590/0370-44672015680058

Salomão F.X.T. 1999. Controle e prevenção dos Processos Erosivos. In: Guerra A.J.T., Silva A.S., Botelho R.G.M. (eds.). *Erosão e Conservação dos Solos: Conceitos, Temas e Aplicações*. Rio de Janeiro: Bertrand Brasil, 340 p.

Salvini F., Storti F. 2001. The distribution of deformation in parallel fault-related folds with migrating axial surfaces: comparison between fault-propagation and fault-bend folding. *Journal of Structural Geology*, **23**(1):25-32. https://doi.org/10.1016/S0191-8141(00)00081-X

Sanderson D.J. 1982. Models of strain variation in nappes and thrust sheets: a review. *Tectonophysics*, **88**(3-4):201-233. https://doi.org/10.1016/0040-1951(82)90237-2

Savage H.M., Cooke M.L. 2004. The effect of non-parallel thrust fault interaction on fold patterns. *Journal of Structural Geology*, **26**(5):905-917. https://doi.org/10.1016/j.jsg.2003.09.006

Schaefer V.R., Mitchell J.K., Berg R.R., Filz G.M., Douglas S.C. 2012. Ground improvement in the 21st century: a comprehensive web-based information system. In: Rollins K.; Zekkos D. (eds.). *Geotechnical Engineering State of the Art and Practice* (No. 226, p. 272-293). ASCE Geotechnical Special Pub.

Schorscher H.D., Santana F.C., Polônia J.C., Moreira J.M.P. 1982. Rio das Velhas greenstone belt and Proterozoic rocks, Quadrilatero Ferrifero, Minas Gerais State. In: International Symposium on Archean and Early Proterozoic Geological Evolution and Metalogenesis, Salvador, Bahia, Brazil, Excursion Annex Book. p. 1-25.

Seeley M., West D.O. 1990. Approach to Geologic Harzard Zoning for Regional Planning, Inyo, National Forest, California and Nevada. *Bulletin of the Association of Engineerind and Geologists*, **27**(1):23-35. https://doi.org/10.2113/gseegeosci.xxvii.1.23

Sepulveda G.O., Novo T.A., Roncato J. 2021. Characterization and geochronology of Archean metasedimentary sequences in the eastern portion of Rio das Velhas greenstone belt, Quadrilátero Ferrífero, Brazil. *Journal of South American Earth Sciences*, **105**:102962. https://doi.org/10.1016/j.jsames.2020.102962

Shamir G., Eyal Y. 1995. Elastic modeling of fault-driven monoclinal fold patterns. *Tectonophysics*, **245**(1-2):13-24. https://doi.org/10.1016/0040-1951(94)00250-D

Storti F., Salvini F. 1996. Progressive rollover fault-propagation folding: a possible kinematic mechanism to generate regional-scale recumbent folds in shallow foreland belts. *AAPG Bulletin*, **80**(2):174-193. https://doi.org/10.1306/64ED8782-1724-11D7-8645000102C1865D

Sullivan W.A. 2013. L tectonites. *Journal of Structural Geology*, **50**:161-175. https://doi.org/10.1016/j.jsg.2012.01.022

Tavani S., Storti F., Salvini F., Toscano C. 2008. Stratigraphic versus structural control on the deformation pattern associated with the evolution of the Mt. Catria anticline, Italy. *Journal of Structural Geology*, **30**(5):664-681. https://doi.org/10.1016/j.jsg.2008.01.011

Teixeira W., Ávila C.A., Dussin I.A., Corrêa Neto A.V., Bongiolo E.M., Santos J.O., Barbosa N.S. 2015. A juvenile accretion episode (2.35–2.32 Ga) in the Mineiro belt and its role to the Minas accretionary orogeny: Zircon U–Pb–Hf and geochemical evidences. *Precambrian Research*, **256**:148-169. https://doi.org/10.1016/j.precamres.2014.11.009

Tricart J. 1961. Lê modele du Quadrilátero Ferrífero au sud de Belo Horizonte. Brésil. Anu. Geograpliie, **379**:255-272.

Vanacôr R.N. 2006. *Sensoriamento Remoto e Geoprocessamento aplicados ao mapeamento das áreas susceptíveis a movimentos de massa na região nordeste do Estado do Rio Grande do Sul*. Dissertação de Mestrado, Universidade Federal do Rio Grande do Sul, Porto Alegre.

Vaz A.L. 2019. Normalizar ou padronizar as variáveis? Available at: https://medium.com/data-hackers/normalizar-ou-padronizar-as-vari%C3%A1veis-3b619876ccc9. Accessed on: Jan 17, 2022.

Xavier da Silva J., Goes M.H.B., Ferreira A.L., Bergamo R.B.A.A., Iervolino P., Rocha E.N., Pacheco E.A., Silveira R.S., Machado R.D., Costa W.P. 1996. Estimativa de riscos de deslizamentos/desmoronamentos no Maciço do Tinguá e Arredores. In: Congresso Brasileiro de Geologia, 39., Bahia. *Anais*... p. 273-276.

Yang R., Jiang D., Lu L.X. et al. 2019. Constrictional strain and linear fabrics as a result of deformation partitioning: a multiscale modeling investigation and tectonic significance. *Tectonics*, **38**(8):2829-2849. https://doi.org/10.1029/2019TC005490

Zhang Z., Thaulow C., Odegard J. 2000. A complete Gurson model approach for ductile fracture. *Engineering Fracture Mechanics*, **67**(2):155-168. https://doi.org/10.1016/S0013-7944(00)00055-2

Zucchetti M., Baltazar O.F. 2000. Rio das Velhas Greenstone Belt lithofacies associations, Quadrilátero Ferrífero, Minas Gerais, Brazil. In: International Geological Congress, 31., 2000, Rio de Janeiro, Brazil. *Anais*... CD-ROM.